CLM - R 176

CLM - R 176

UKAEA

Report

SURVEY OF TOKAMAK EXPERIMENTS

R J BICKERTON

CULHAM LABORATORY
Abingdon Oxfordshire
1977
Available from H. M. Stationery Office
C.18
£2.00

CLM - R 176

SURVEY OF TOKAMAK EXPERIMENTS

LECTURES GIVEN AT INTERNATIONAL SCHOOL OF PLASMA PHYSICS

VARENNA, SEPTEMBER 1977

by

R. J. BICKERTON

(Euratom/UKAEA Fusion Association)

ABSTRACT

The survey covers the following topics:-

Introduction and history of tokamak research; review of tokamak apparatus, existing and planned; remarks on measurement techniques and their limitations; main results in terms of electron and ion temperatures, plasma density, containment times etc. Empirical scaling; range of operating densities; impurities, origin, behaviour and control (including divertors); data on fluctuations and instabilities in tokamak plasmas; data on disruptive instabilities; experiments on shaped cross-sections; present experimental evidence on β limits; auxiliary heating; experimental and theoretical problems for the future.

UKAEA
Culham Laboratory
Abingdon
Oxon, England

SBN 85311 059 X

CLM-R 176

Corrigenda

Survey of Tokamak Experiments

Lectures given at the International School of Plasma Physics, Varenna, September 1977

by

R J Bickerton

(Euratom/UKAEA Fusion Association)

Page	Line	
3	8	After "1.4 x 10^{13} cm^{-3}" add "s.keV".
12	16	Alter "increase" to read "increased"
12	17	Alter "B_ϕ" to read "β_ϕ".
14	27	Alter "$t = \frac{10^{11}}{800} n$——" to read "$\Delta t = \frac{10^{11}}{800} n$——".
15	7	Alter ΔT to read Δt.
34	10/11	Alter "current" to read "density".

UKAEA
Culham Laboratory
Abingdon
Oxon, England

February 1978

SBN 85311 059 X

REVIEW OF TOKAMAK EXPERIMENTS - PART I

1. INTRODUCTION

The purpose of this review is to give an account of the results of tokamak experiments. I am not attempting a comprehensive treatment of tokamak physics; this is well covered in the review articles by Artsimovich[1] and Furth[2] while the hydromagnetic stability theory will be dealt with in detail in other lectures at this School.

Nevertheless I would like to discuss briefly the history and evolution of the tokamak. The story began in the mid-1950's when it was realised more or less simultaneously in the USSR, USA and UK that the addition of a toroidal magnetic field to a toroidal pinch would improve the stability of the discharge against the simplest amd most dangerous modes. The combination of the self-magnetic field of the plasma current and the externally produced toroidal field gives helical field lines and a very important tokamak parameter, the 'safety factor' q is simply the number of times a field line circles the major axis in circling once around the minor axis. The most dangerous remaining unstable modes tend to be those in which the perturbation helix matches the field helix since this results in the minimum change of magnetic energy. That is perturbations of the form

$$\xi = \xi(r)\ \mathrm{expi}(m\theta + n\phi) \qquad .. (1)$$

where the coordinate system is defined in Fig.1 and

$$\frac{m}{n} = q \qquad .. (2)$$

Early theoretical work showed essentially two classes of magnetically stabilised pinches. The first (tokamak) in which stability against the dangerous low order (m=1, n=1) mode is achieved by <u>geometric</u> means, i.e. by making $q > 1$ at all radii in the discharge, and the second in which $q < 1$, with stability achieved by shear and a conducting wall close to the plasma ('stabilised pinch','diffuse pinch' 'reversed-field pinch'). Since from the geometry of field lines and for circular cross-section magnetic surfaces,

$$q = \frac{r}{R}\frac{B_\phi}{B_\theta} = \frac{r^2}{2IR}B_\phi \qquad .. (3)$$

where r is the minor and R the major radii of the magnetic surface, it is clear that the tokamak system requires a much larger externally applied field B_ϕ than does the stabilised pinch. Thus it was that in the mid-

1950's the USA and UK concentrated on the apparently cheaper stabilised pinch leaving the tokamak approach to the Soviet Union.

The early Soviet work was initiated by Yavlinski and Artsimovich and was a struggle to solve two main problems, discharge cleanliness and measurement methods. Adequate purity was gradually achieved by progression from insulating toruses to metal ones and finally to metal ones with refractory metal limiters to reduce wall damage. The problem was to measure key parameters such as electron and ion temperatures, and this very difficulty compounded the problem of convincing plasma physicists generally of the virtues of the system. Thus the plasma energy content could only be established by diamagnetic loop measurements, the analysis being complex and unconvincing but as it turned out - correct. Success was measured very largely in terms of increasing the plasma electrical conductivity; in parenthesis we note that even today the simplest test of successful tokamak operation remains that of getting the loop voltage down to a few volts per turn, i.e. getting high conductivity.

Towards the end of the 1960's the broad features of tokamak design and performance as we know them today had been established[3]. The main elements of a standard tokamak were as shown in Fig.2, in particular an iron core, metal-walled torus, tungsten or molybdenum limiter, copper stabilising shell, vertical field windings and toroidal field coils. Performance features noted by then included the disruptive instability when q at the limiter < 3, the limited range of operating density between excessive runaway at low values and disruption at high density, the electron temperature from X-rays or diamagnetism as typically $4 \div 5$ times the conductivity temperature, the major radius equilibrium of the plasma in agreement with theory and energy containment for substantially longer than the Bohm time.

Outside the Soviet Union the tokamak was regarded as inflexible and difficult to understand because of the coupling between heating and containment and difficult to diagnose because the plasma was hidden behind relatively massive toroidal field coils. Then in 1969, as a result of an initiative by Pease and Artsimovich, Thomson-scattering measurements carried out on T3 by a joint Culham/Kurchatov team showed beyond question that all the claims for the performance of the system were fully justified[4].

This success, coupled with a marked lack of success in other systems led to a rapid and worldwide concentration on the tokamak system. In the last seven years the main effort on fusion by magnetic confinement has been on the tokamak, and great advances have been made both in parameters achieved and in understanding. Plasma currents have been taken from the 1969 level of 150kA

to ~600kA in PLT, energy containment times from 10 ms to 50 ms, ion temperatures from 600eV to ~2keV, while peak electron temperatures have remained relatively static at 1 - 2keV. Sample current-voltage traces from the 1969 T3 and the 1976 T10 are shown in Fig.3. These historical advances are summarised in Fig.4 in terms of the key Lawson parameters $\langle n\tau_e \rangle$ and T_i. It should be emphasized that the figures for 1977 are not obtained simultaneously in the same discharge, probably the best value for $\langle n\tau_e \rangle . T_i$ in a single shot is ~$1.4 \times 10^{13} cm^{-3}$ What is most remarkable is that this peak achievement is obtained in a discharge (Alcator) with a current of only the same order (~100 kA) as that in the 1965 T3 tokamak.

2. TOKAMAK APPARATUS

TABLE I is a list of representative tokamak devices. Fig.5 produced by the JET group, shows to scale the cross-sections of some of the systems. Striking is the small physical size of Alcator. Note that some have dispensed with the traditional iron core and thick conducting shell. An air-cored transformer enables a larger flux swing to be used than the limit of 35 kG from iron; the disadvantages are the need for more energy from the driving power supply and the problem of ensuring a small enough stray field inside the torus. Very roughly for a small aspect ratio torus the flux swing in the transformer must be at least of the same order as the toroidal field so that an air core is obligatory in high field machines such as Alcator. A hybrid variant is the proposed JET device which has an iron core, but one in which the central limb is well saturated while the outer limbs are not. This gives some energy saving, largely solves the stray field problem and the iron in the centre is also useful from a structural viewpoint. The role of the conducting shell is twofold. It provides through eddy currents the vertical magnetic field needed to give major radius equilibrium to the plasma toroid[5]. It also assists in stabilising helical plasma modes by requiring the perturbed magnetic field normal to the conductor surface to be zero. A typical copper shell approximately 2.5cm thick has a time constant for the equilibrium role of order 50 ÷ 100 ms. Thus for longer duration discharges typical of today's machines it is necessary anyway to provide a vertical field with external windings. Dispensing with the conducting shell enables a larger minor radius torus to be used within the same toroidal field coils, thereby increasing the current capacity of the device at constant q (equation 3). It is essentially this modification that has recently converted TFR 600 from 400 kA to ~600 kA.

Although a stable equilibrium can in principle be provided for circular cross-section machines by a passive vertical field system[5] most of those without conducting shells use a feed-back arrangement with magnetic or optical detection of the discharge position. With shaped cross-sections feed-back becomes increasingly necessary rather than just desirable.

The majority of devices use water-cooled, copper toroidal field coils but for very high toroidal fields the required current density can only be achieved with liquid nitrogen-cooled copper. Ormak and DITE, both relatively low field systems, also use liquid nitrogen-cooled coils, the former to obtain a small aspect ratio, the latter because of the limited power presently available at Culham. A disadvantage of these cryogenic systems is the cool-down time between pulses, ~20 minutes at full field in the DITE case. This is frustrating for experimentalists and may actually change some features of the plasma-wall interaction. A superconducting tokamak (T7) is in an advanced stage of construction in the Soviet Union and another (Torus II) is being designed in France. The outstanding difficulty here is the shielding of the superconductor against pulsed poloidal fields. It is not clear to me whether the use of superconductors is a cheap and effective way of building an apparatus, or whether building in this way is in itself a technical experiment.

The principal engineering problems in building tokamaks come from the large magnetic forces involved, the main ones being the inward force on each toroidal field coil (~1800 tonne in JET) and the torque on each coil due to interaction with the vertical magnetic field (~200 tonne metres in JET)[6]. These forces must be transferred from the copper-insulator laminate of a typical coil to the restraining structure. The limiting factor is the permissible stress in the insulator and in the next generation of machines the problem will be compounded by neutron radiation damage of that insulation.

3. PLASMA MEASUREMENTS

The measurement of current and loop voltage is straight-forward although there may be difficulties in deriving the resistive component of voltage, i.e. making proper allowance for inductance and current changes. The electron density (r,t) and temperature $T_e(r,t)$ are most reliably measured by Thomson scattering. The technique is tedious in the sense that there are typically only $1 \div 4$ laser pulses of short duration (~25 ns) during a discharge pulse giving $1 \div 4$ time resolved measurements at one point in the plasma. Thus to build up radial profiles requires many pulses and good plasma reproducibility. Using a high brightness laser, and complex detection systems, it is now possible to measure the parameters at several radial positions from a single

laser pulse (as on PLT and planned for TFR 600). The electron temperature can be continuously measured as a function of time by analysis of the soft X-ray emission. This is a chordal line of sight measurement and requires some unravelling to give $T_e(r,t)$; a good simple interpretation is that it measures the highest temperature in the sight line. Another new and very useful method which gives $T_e(r,t)$ with about 10 ms time resolution and approximately $^a/_5$ space resolution is through analysis of the electron cyclotron emission, usually the line shape at the second harmonic. The measurement is made along the major radius, the spatial resolution comes from the variation of the toroidal field strength and hence the emitting frequency while the intensity is taken to be the Rayleigh-Jeans level for the local temperature. Both this and the X-ray method gain credibility, and sometimes calibration, by comparison with the Thomson scattering data. The electron density $n_e(r,t)$ is also obtained by Abel inversion of multi-channel microwave interferometer measurements. This technique has recently been extended to shorter wavelengths (and therefore to higher densities before refraction and cut-off difficulties) through the use of an HCN laser source at 337 μm.

The ion temperature is measured by analysis of the fast neutral atoms leaving the plasma. These originate in charge exchange collisions between plasma ions and neutral atoms inside the plasma. Again the method is a line of sight one and again the temperature deduced from the higher energy end of the spectrum is likely to correspond to the highest value in the line of sight. Fig.6 shows a typical spectrum from DITE. There is a high intensity at low energy believed to come from charge exchange near the walls where the ion temperature is low and the neutral density high. The higher energy part gives a linear plot on semi-log representation corresponding to a Maxwellian; the temperature is then assumed to be the highest in the sight line. Note that one is typically measuring ions from well up in the Maxwellian tail, $\epsilon_i/T_i \sim 5 - 10$. Radial resolution is obtained by measuring along different chords and the time resolution is typically 10 ms. The method breaks down in high $\overline{na}$ machines because fast neutrals from the centre are re-ionised before they reach the wall. This has been strikingly demonstrated in Alcator where the emission of fast neutrals simply drops below the detection threshold as the average plasma density rises through $1.5 \times 10^{14} cm^{-3}$. The ion temperature can be checked (or measured?) using the neutron yield from deuterium discharges. This of course depends on discriminating between photo-neutron and thermonuclear neutron production and on the maintenance with present ion temperatures of a strictly Maxwellian ion velocity distribution out to

approximately 10 or more times the mean energy. New methods of ion temperature measurement are badly needed. Possibilities include far infra-red (collective) scattering, in which a clear interpretation depends on a thermal level of ion sound fluctuations, Doppler broadening of H_α, L_α and of resonance impurity lines.

A check on the measured profiles of n_e, T_e and T_i is provided by the measurement of plasma diamagnetism. A further cross-check can be obtained from the outward shift of the column in a conducting shell system, or equivalently, from the required vertical field in a feedback system.

External magnetic pick-up coils are used to detect hydromagnetic modes (m = 2,3,4 ....) which perturb the field outside the plasma. Internal fluctuations of electron temperature are detected by space and time resolved soft X-ray measurements. Local fluctuations of electron density can be measured by microwave or CO_2 laser light scattering ($k\lambda_D \ll 1$).

The neutral density inside the plasma is normally calculated by Abel inversion of chordal measurements of the intensity of H_α emission. This is inaccurate near the discharge centre because of the intense emission from the outer regions and its effect on the Abel inversion. The neutral density can also be deduced through its effect on the spectrum (through charge exchange) of fast injected ions. A promising method yet to give a result is that of L_α resonance fluorescence using a tunable laser source. This has the advantage of giving a spatially resolved measurement, and by tuning the laser across the line the Doppler broadening and hence the neutral temperature should also be measurable. The general technique of fluorescent spectroscopy using tunable lasers on impurities as well as hydrogen should be a rewarding field in the future.

It is important to measure the concentration of impurity atoms in the plasma and if possible to deduce their life history. Impurities reaching the hotter regions become multiply-ionised and their primary emission lines will typically be in the wavelength range corresponding to $1 \div 5$ times the mean electron temperature. Bearing in mind the range of temperatures from the wall to the axis we see that we are dealing with emission spectroscopy from the visible, through the normal and grazing incidence regions to the soft X-ray crystal spectrometer region. Absolute calibration is difficult in the shorter wavelength regions and even when the intensity is known a theoretical model must be used to deduce the impurity concentration. The charge state of impurity ions can be deduced from the shift of K_α lines and their temperature from

the Doppler broadening.

The energy lost in the form of radiation and neutral particles is measured by bolometers at the wall of the torus. The radial dependence of the loss is again deduced by Abel inversion of collimated chordal measurements. The calibration of these detectors is difficult and the accuracy often little better than 50%.

After all these years of tokamak research it is perhaps astonishing that we still have no direct and convincing way of measuring the radial variation of the current density or equivalently the poloidal magnetic field. The current density profile is paramount in the theory of the hydromagnetic stability of tokamaks and yet so far we cannot measure it. At present it is calculated by assuming that $j_\phi \propto T_e^{\frac{3}{2}}$ and that Z_{eff}, the effective charge of the plasma ions is uniform across the discharge radius. Many methods for measuring the poloidal field have been proposed, and some have yielded primitive results, but none have yet given data of sufficient quality to be used in a serious analysis of the discharge. They include measuring the trajectories of fast injected ions, the polarisation of microwaves and the Zeeman effect. At Culham we are concentrating on a light scattering method[7]. This uses the fact that because of the low beta and high q in existing machines we know the <u>strength</u> of the local magnetic field quite accurately, the poloidal field has an influence only on the direction of the field. Now the Thomson scattered spectrum for scattering vectors sufficiently near perpendicular to the local field is modulated at the electron cyclotron frequency. Hence by measuring the scattering angle at which the modulation occurs we can deduce the poloidal field.

I hope that I have said enough about diagnostics to convince you of their difficulty, their importance and their inadequacy. They are often inaccurate and depend on assumptions which are difficult to prove. Consequently it is a good general principle to measure every parameter by at least two methods and to treat all results with initial disbelief. We cannot have too many measurements and as we shall see later the quantity and quality of data on existing machines is very, very rarely enough to enable a detailed comparison with theory to be made.

4. <u>COARSE CONFINEMENT AND SCALING</u>

The basic question about tokamaks is whether they can eventually contain plasma to satisfy the reactor criteria for the Lawson parameters $n\tau_\varepsilon$ and T_i in apparatus of sufficiently moderate size to be of practical and economic

interest.. Or to put the question another way, how far do we have to scale up on the existing range of machines to obtain reactor performance. To answer this we can try to understand the detailed workings of existing machines, to understand the influence of moving into new regimes of various dimensionless parameters (e.g. ratio of collision to bounce frequencies, β etc) and so to extrapolate to the reactor regime. We can also adopt a somewhat different line, that is to see whether we can establish from the existing data an empirical scaling law. Of course if we can find one we have no right to expect that the same law will continue to hold over the decades of parameter space that we still have to cross to reach the Eldorado of the reactor regime. However as we shall see there is some interest in this approach.

The search for such a law is not new. From the early Soviet work two laws were proposed[8],

$$\tau_\epsilon \propto a^2 n_e T_e^{\frac{3}{2}} \qquad ..(4)$$

$$\tau_\epsilon \propto a.I \qquad ..(5)$$

while more recently Daughney [9] proposed on the basis of a wider data set the law,

$$\tau_\epsilon \propto \frac{\bar{n}_e a^3 T_e^{\frac{3}{2}}}{Z_{eff}^{\frac{1}{2}} I^{\frac{3}{2}}} \qquad ..(6)$$

The energy containment time τ_ϵ referred to here is simply defined as

$$\tau_\epsilon = \frac{Wp}{VI} \qquad ..(7)$$

$$\tau_\epsilon = \frac{4.7 \times 10^{-2} R \int_o^a 2r (n_e T_e + n_i T_i) dr}{VI}$$

where Wp is the total plasma energy and VI is the power input in steady state.

The most recent and most systematic analysis has been carried out by Hugill and Sheffield[10]. They assume that the containment time can be expressed by the form,

$$\tau_E = \exp(x_1) a^{x_2} . b^{x_3} . c^{x_4} \quad .. \qquad ..(8)$$

where a,b,c, ... are various machine and plasma parameters. For a set of n experimental results this gives n equations of the form,

$$\log \tau_E = x_1 + x_2 \log a_i + x_3 \log b_i + \ldots \qquad ..(9)$$

or $$y_i = \Sigma_j A_{ij} x_j \quad \text{where} \quad i = 1, \ \ldots \ n$$

These form an overdetermined set of linear equations for which a solution $\bar{x}_j$ is found which minimises $\Sigma_i (y_i - \Sigma_j A_{ij} x_j)^2$.

To quantify the significance of the result they calculate the correlation function,

$$R_c = \frac{\Sigma_i (z_i - \bar{z}_i)(y_i - \bar{y})}{(\Sigma_i (z_i - \bar{z})^2)^{\frac{1}{2}} (\Sigma_i (y_i - \bar{y})^2)^{\frac{1}{2}}} \qquad ..(10)$$

where $z_i = \Sigma_j A_{ij} \bar{x}_j$.

The data set used for this work is shown in TABLE 2 and is in any case a useful collection of results. To use the technique a decision has to be made as to which of the plasma and machine parameters to use in the scaling. The results of a variety of choices are shown in TABLE 3, together with the resultant correlation coefficients. The 'trial 1' scaling is shown plotted in Fig.7. The scaling shown was deduced without using the data from T10 and PLT. The results from those machines given at the Berchtesgaden conference are plotted on the graph and agree in a gratifying way with the predictions of the scaling law. All the data corresponds to discharges with only ohmic heating. In fact no experiment has yet operated with an auxiliary heating power greater than the ohmic input. Ohmic heating with classical resistivity introduces a coupling between the electron temperature and the containment time of the form,

$$\tau_\varepsilon = \frac{(\text{const}) \ n T_e^{\frac{5}{2}} \ r^4}{I^2} \qquad ..(11)$$

Taking this equation with the empirical scaling law (trial I, say),

$$\tau_\varepsilon = 2.7 \ \bar{n}_e^{0.61} \ a^{1.57} \ B_\phi^{0.88} \ A_i^{0.65} \ \text{ms} \qquad ..(12)$$

where $\bar{n}_e$ is in units of 10^{13}cm^{-3}, a in metres and B_ϕ in kGauss it is possible to predict both the temperature and the energy containment time for future devices with ohmic heating. These predictions are shown in TABLE 4. The temperatures foreseen are similar to but slightly lower than those in present devices and the authors conclude that this emphasizes the need for powerful auxiliary heating if higher temperatures are to be reached.

Stimulated by this empirical scaling work Taylor and Connor [11] have recently considered the limits imposed on the scaling indices $x_1, x_2, \ldots$ if it is assumed that the plasma behaviour is <u>determined entirely by plasma physics</u>.

As an example if the plasma physics is based on one plasma model, say the collisionless Vlasov equation, then that basic equation must be invariant under the transformations represented by the scaling laws. This leads to restrictions on the indices. In the Vlasov case the restriction is so strong that for diffusive phenomena only the Bohm scaling is possible. For more general models such as the collisional Vlasov equation, the resistive fluid etc., there is more freedom but the indices are still required to satisfy certain relationships. Taylor and Connor show that the indices deduced by Hugill and Sheffield do not satisfy these requirements. There are at least two possible conclusions. One is that the attempt to force the results into a power law form is misguided. Clearly if the plasma physics regime changes (e.g. in the various regimes of neo-classical theory or of trapped particle modes) then a power law form is inappropriate. The Taylor/Connor work still puts limits on the functional form of the (non-power law) relation - attempts to look at the data in this light show that there is not enough data. A second conclusion is that factors other than plasma physics are involved in the scaling. Obvious ones are radiation and charge exchange losses. If we had enough data to subtract these losses so as to be left with a residual $(\tau_E)_p$, i.e., an energy containment time determined by plasma physics, then the resulting scaling would have to satisfy the Taylor/Connor conditions.

The overall conclusion would seem to be that we cannot expect to 'explain' the present results on the basis of plasma physics alone and that if we are to make progress in that direction we need much more detailed measurements of as wide a range of discharges as possible. Another point which has long been recognised is that we can only obtain decisive information on temperature scaling when we can use auxiliary heating power comparable with or larger than the ohmic input. This is expected to be achieved shortly in at least three experiments, PLT, TFR and DITE. On DITE for example we expect to have in excess of 1 MW of injection power into the plasma compared with the present ohmic input of approximately 500 kW.

REVIEW OF TOKAMAK EXPERIMENTS - PART II

1. INTRODUCTION

In the next part of my review I will be discussing the experimental results from tokamaks in greater detail. To give some structure to the discussion I will divide the subject matter under various headings but I would emphasize the overlapping nature of the subject. Thus the disruptive instability is related to impurity content and influenced by auxiliary heating etc., etc.

2. PLASMA EQUILIBRIUM

Most tokamak data refers to systems with the relatively high aspect ratio ($R/a > 4$), near-circular cross-section magnetic surfaces and $\beta_\theta < 1$ (where $\beta_\theta = \frac{2\int_o^a 2\pi r\,(n_e T_e + n_i T_i)dr}{I^2}$). The agreement with equilibrium theory [5] is then good in respect of the major radius equilibrium. That is to say, shifts within conducting shell systems or equivalently the applied vertical field in the non-shell devices are consistent with expectation. Since there are no measurements of $j_\phi(r)$ and $j_\theta(r)$ the minor radius equilibrium is not directly checked. But the relatively long particle and energy containment times observed ($\gg a/c_s$ where c_s = plasma sound speed) are convincing demonstrations that the plasma is in pressure equilibrium with the field. Anomalous major radius shifts seen in early work on TM3 were almost certainly correctly ascribed to the presence of a large runaway electron component in the plasma. So far only a few 'scouting' experiments have been made into the regime $\beta_\theta > 1$. First on T3 and later on ST, β_θ was taken to $7 \div 8$ by suddenly reducing the discharge current on a timescale short compared with the energy containment time. The plasma remained in equilibrium, but the nature of the equilibrium can be questioned since the current change was also fast compared with the field penetration time for the column. In other terms the role of flux conservation and of surface currents in those experiments is not known. In the small Russian tokamak TO-1 (R = 60 cm, r = 18 cm, I ~ 15 kA) magnetoacoustic heating was used to increase β_θ transiently to ~ 1.2[12]. Similarly high powered electron cyclotron heating was used to increase β_θ to ~ 2.3 in the TM-3 machine running at the low toroidal field strength of 5 kG [13]. The most convincing high β_θ experiments have been those on Alcator[14], and Pulsator[15] (Fig.8) where in the high density mode ohmic heating alone produces $\beta_\theta \sim 2$, limited by disruption

at higher density.

The evidence from these preliminary experiments is encouraging although no experiment has yet demonstrated clearly the equilibrium limits to β_θ. The ohmic heating experiments are limited by disruption at the higher densities and as we shall see later we believe this effect to be unrelated to the β_θ value as such. Much more information on equilibrium limits should come from the next phase of experiments in which the auxiliary heating (in particular neutral injection) will be several times more powerful than ohmic heating.

In the long term the key parameter is not β_θ but $\bar{\beta}$ where $\bar{\beta} = \dfrac{\overline{8\pi n_e (T_e + T_i)}}{B_\phi{}^2}$ averaged over the plasma volume or, arguably in the reactor case, over the plasma plus blanket volume. For given safety factor (q), $\bar{\beta}$ can be increased by going to a non-circular cross-section, usually one elongated in the direction parallel to the major axis of the toroid. The increase in $\bar{\beta}$ results from the increase in the ratio of the peripheral length (ℓ_1) round the minor cross-section of the plasma to the length of the magnetic axis, and hence of the ratio B_θ/B_ϕ. For given β_θ this then gives increase β_ϕ, since

$$B_\phi = \beta_\theta \cdot \left(\frac{\ell_1}{2\pi R}\right)^2 \frac{1}{q^2} \qquad ..(13)$$

The Doublet[16] series of experiments at San Diego are with the most extremely elongated of conventional tokamaks and encouraging results have been obtained with the IIA device showing a marginally higher β_ϕ (Fig.9) with an elongation of 2.9 and a substantial increase (sevenfold) in the containment parameter $\langle n\tau_\epsilon \rangle$ compared with elliptical cross-section. A recurring difficulty with this type of experiment is to know what to keep constant in comparing the elongated and near-circular cross-section cases.

Reactor designers require $\bar{\beta}$ values in excess of 5% if the system is to be economic. This is much higher (x 10) than the best achieved in existing machines. Theoretically the flux conserving tokamak concept [5,17] shows that in principle very high values of $\bar{\beta}$ are possible as equilibria with safety factor (q) values comparable to those in present devices. The key questions are whether these equilibria are sufficiently stable and whether they can be maintained for long enough to be useful. An experimental test of this idea will require very high auxiliary heating power. Consider for example the DITE tokamak; it has a plasma volume of $1.2 \times 10^6 cm^3$ and a maximum toroidal field at 28 kG. Thus for a $\bar{\beta} \sim 10\%$ averaged over the plasma volume the required plasma energy is 0.6 MJ. To put this in on the time scale of the present

energy containment time (20 ms) would require an input power (P_1) of 30 MW. If we make the more optimistic assumption that $\tau_\epsilon \propto n$, and that (with Murakami) $n_{MAX} \propto P_1$, then the required power is given by

$$P_1^2 = 30 \cdot P_\Omega (MW)^2$$

where P_Ω is the present ohmic input power and taking for DITE

$$P_\Omega = \frac{1}{2} \text{ MW},$$

we find $P_1 = 4$ MW (corresponding to $\tau_\epsilon = 160$ ms!)

Thus it may be possible to test the high $\bar{\beta}$ concept at low temperature and high density with neutral injection heating powers which are just feasible by today's standards of technology.

In the long term it seems likely that a combination of a perhaps mildly elongated cross-section and an equilibrium of the flux conserving type without excessive variations of the toroidal current density will enable adequate values of $\bar{\beta}$ to be sustained in quasi steady state.

3. FLUCTUATIONS IN TOKAMAK PLASMAS

Early evidence of fluctuations in tokamak plasma was obtained by Mirnov [18] using magnetic pick-up coils outside the plasma column. Fig.10 shows a typical set of results which shows the evolution of $n = 1$, $m = 6,5,4 \ldots$ magnetic perturbations (Mirnov oscillations) as the current increases and the safety factor at the limiter falls below these values. These are now interpreted as the external manifestation of tearing modes centred on the appropriate resonant surfaces $m/n = q$ inside the plasma. The amplitude of the oscillations can reach $\sim$ 20% of the mean poloidal field. Mirnov oscillations of $m = 2$ are usually soon followed by a 'disruptive' instability in which there is large negative spike, a substantial and sudden reduction in the energy content of the plasma, a sudden change in the major and minor radii of the plasma and in extreme (hard) disruption complete extinction of the discharge current. Fig.11 shows the current and voltage traces for soft and hard disruptions taken on the Pulsator [19] tokamak. In general disruption occurs if q at the limiter is too low or if the plasma density is too high. Work on T3, T4 and T6 showed that the value of q at the limiter could be reduced without disruption the nearer the conducting shell was to the plasma. With the shell close to the plasma boundary the Mirnov oscillations tend to be confined to bursts as q(limiter) goes through integral values. By programming the current to pass rapidly through the resonances, 'stable' discharges with $q < 3$ could be obtained. The sensitivity to the

shell position can be gauged from the fact that T4[20] could be operated with $q \sim 2$ much more readily than T3; the shell in the first case was at a radius of 23 cm compared with 25 cm in the second[20]. The plasma confinement in these grossly stable modes of operation with low q has been found to be relatively poor and this has meant a pronounced lack of enthusiasm for low q operation in recent years. Fig.12 shows this result very clearly for T3. The energy containment time is largely independent of the toroidal field strength until the current exceeds the level at which q (limiter) ~ 3. Further increase in the discharge current leads to a rapid reduction in confinement time.

Striking evidence of internal fluctuations[21] has been obtained by collimated, chordal, soft X-ray measurements. A typical experimental arrangement is shown in Fig.13. The soft X-ray detectors are effective for the energy range $4 \div 5$ keV typically. The X-ray emission in that range from a thermal plasma would be expected to depend on the electron density, the electron temperature and the impurity content. The X-ray signals from the centre of the plasma show a characteristic sawtooth behaviour. A typical result from TFR[22] is shown in Fig.14. The signals consist of two basic parts, the main relaxation oscillations which can be shown by correlation of signals from different azimuths to be of $m = 0$ mode and the high frequency part which similarly is shown to be $m = 1$. The relaxation part reverses phase at a radius r_o where it is believed that $q = 1$. The value of r_o determined from phase reversal agrees roughly with that determined by measuring $T_e(r)$ and assuming that $j_\phi \propto T_e^{\frac{3}{2}}$. Using the notation shown in Fig.14 the TFR group established the empirical relations,

$$r_o = \frac{0.5a}{(q(a))^{\frac{1}{2}}}$$

$$t = \frac{10^{11}}{800}\, n(0) r_o^{\,2} R \qquad ..(14)$$

$$\left[\frac{\widetilde{\Delta A}}{A}\right] = \frac{1.5}{(q(a))^{\frac{3}{2}}}$$

The interpretation of these X-ray signals has proved quite complex and is still not conclusively settled. From Thomson scattering and spectroscopic measurements the TFR group conclude that the X-ray fluctuations are due mainly to variations in the electron temperature. They conclude that on the axis of the discharge $\Delta T_e/T_e \sim 10\%$ while $\Delta n_e/n_e \sim 1 - 2\%$ only. On the other hand the simple corollary that $\frac{\Delta A(r)}{A} = \text{const.}\, \frac{\Delta T_e(r)}{T_e}$ leads to the difficulty that after a relaxation the energy gained in radii $> r_o$ then

exceeds that lost from the zone $r < r_o$. To avoid this difficulty it is necessary to postulate that the fast electrons are decoupled from the plasma on the fast time scale δt so that the observations of the fast phase are not representative of the bulk of the electrons. The Oak Ridge[23] group arrived at similar conclusions when they measured an effective thermal conductivity by studying the time behaviour of the 'temperature' pulse in the outer regions. The rise in the central X-ray signal over the long time scale ΔT is consistent with the ohmic heating rate there. Thus the picture is of the central region $r < r_o$ heating up while that with $2r_o > r > r_o$ cools down, there are growing $m = 1$, $n = 1$ oscillations some sudden phenomenon on the scale δt which redistributes the energy to the outer zone, then the whole cycle begins again. This relaxation phenomenon dominates the energy balance in the central regions. These internal so-called mini disruptions are now widely interpreted as due to $n = 1$, $m = 1$, kink modes which are unstable whenever $q(0) < 1$. Supporting evidence for this comes from the observation that sawtooth oscillations are not seen when from the temperature profile and $j \propto T_e^{\frac{3}{2}}$ assumption $q(0) > 1$. It is of course necessary to invoke some non-linear consequence of the kink mode such as magnetic surface break-up to 'explain' the observations. Interpretations of the signals in terms of electrostatic rather than hydromagnetic modes have been offered but have not gained wide acceptance. Curiously, sawtooth oscillations are not seen in clean high density discharges in Alcator[14], though they are seen in the Pulsator high density work. The oscillations <u>do</u> occur in Alcator after a disruption at the limiting density. This evidence would suggest that impurities have more to do with the signals than is commonly assumed.

Armed with the ability to measure both internal and external fluctuations, it is possible to make a detailed study on a fast time scale of the phenomena just before and during a disruptive instability. Such studies have been made on several machines, notably Pulsator[19] and T4[24]. In Pulsator signals from the soft X-ray diodes, loop voltage, discharge current and external pick-up coils were measured on a fast time scale before disruption using a multi-channel transient recorder. Approximately 10 ms before the disruption the $m = 2$ oscillations detected on coils start to grow in amplitude and cycle duration imposing their frequency on the $m = 1$ internal mode detected by soft X-ray diodes. After coupling, the amplitude of the oscillations grows faster and the frequency continues to decrease until immediately before the negative voltage spike. At this time the fast records (Fig.15) show the superposition of a phase-locked $m = 1$ mode in the interior with an $m = 2$ mode

outside. The temperature maxima of the m = 2 mode coincide with the current maxima as measured by the poloidal field coils. The authors conclude that the signals represent the uniform toroidal rotation of a rigidly coupled system of m = 1, n = 2 and n = 1 perturbations. The system rotates in the direction of electron drift. After the perturbations have reached a certain amplitude, immediately before the negative voltage spike, very hard X-rays (E > 1 MeV) are emitted from the limiter. These X-rays are emitted in bursts synchronised with the rotation of the helical system and occurring when a given point in the coupled helices passes the limiter. After the main burst the temperature in the plasma interior decreases significantly (Fig.15). The resolving power of the diodes is 15 μs. In separate experiments with 1 μs diodes it is shown that the temperature drop occurs 10-20 μs before the leading edge of the negative voltage spike. The negative voltage spike is accompanied by a positive spike in the plasma current and a fast inward (major radius) motion of the plasma. Pulsator is equipped with a helical winding m = 2, n = 1. By passing current through this winding, disruptive instabilities can be triggered when the sense of the helix is the same as that of the tokamak magnetic field and when the winding current exceeds a certain threshold which increases with q. The influence of this winding on q is negligibly small ($^{\delta q}/_{q} \sim 10^{-5}$) and it is believed that the main effect is due to the creation of magnetic islands on the q = 2 surface as a result of the resonant perturbing field. If the helical winding current is just below the threshold for disruption there is a stabilising effect, hard disruptions which would otherwise occur being delayed or avoided. Disruptions produced by large external winding currents show no precursor $m = {}^{2}/_{m} = 1$ activity, except between the X-ray burst and the disruption.

The authors infer the following sequence for the disruptive instability; "the coupled m = 1 and m = 2 modes impose a growing, rotating helical structure on the drift surfaces of the runaways which has a fixed phase relation to the magnetic island system. Runaways are displaced outwards with respect to surfaces by typically 1.5 cm for 6 MeV. Following the growth of the perturbation, deeper and deeper layers of runaways are depleted at each rotation. As the perturbations grow so do magnetic islands and eventual 'ergodisation' of the field lines leading to a sharp reduction in the temperature in the interior. The corresponding reduction in β_θ causes the plasma to be pushed inwards in major radius by the vertical field, causing a positive spike on the current and a negative spike on the loop voltage. The calculated and observed inward displacement could at best only explain the magnitude of the first step on the negative voltage spike. One has to assume an additional reduction in

the plasma inductance corresponding to an expansion in minor radius of the current channel to account for the full value of the negative voltage spike. Such an expansion is consistent with the increase of H_α and fast neutral flux at the instant of the leading edge of the negative voltage spike".

The disruptive instability studied in this Pulsator work is triggered at constant plasma current by rising plasma density. By contrast the T4 study is of a disruption produced by a programmed rise in the plasma current, i.e. a decrease in the limiter q. The T4 workers found that the disruption has a complex time structure, i.e. its initial phase is always a pre-disruption during which the helical perturbation m = 2 propagates from the boundary into the interior followed by a symmetric expansion of the central region (m = 0) with simultaneous development of m = 1 at the centre. This is followed by the final stage - a violent burst of m = 2 activity which then becomes m = 3 and m = 4 probably due to the fast expansion to the walls and the consequent increase in q at the plasma edge from 2 to 4. Fig.16 shows the signals recording plasma current, loop voltage, perturbed poloidal field and soft X-ray emission before and during a disruption. The sharp drop in central temperature just before the negative voltage spike is clearly seen. The dotted lines show the parameter variation in the case when pre-disruption activity does not lead to a disruption. The sequence of events finally inferred by the T4 group is

"1. Slow compression of the current channel, decrease in q(0) to 1 and q(a) to $\sim$ 2.

2. Rapid development of m = 2 near boundary, with the formation of magnetic islands.

3. Destabilisation of m = 1 near centre due to q(0) < 1 or deterioration of stabilising properties of the periphery.

4. Mixing of m = 1 and m = 2, flattening of j(r), increase of q(0) to 1.5.

5. Disruption per se. Violent non-linear development of m = 2 in the present of flattened j(r). Turbulisation of the column, its expansion to the walls of the discharge chamber with corresponding transformation of m = 2 into m = 3 and m = 4 perturbations".

It is interesting to note that from the amplitude of the m = 2 perturbations in the poloidal field the T4 group infer the existence of locally reversed toroidal currents in the outer regions. They argue that the collapse of

these currents may be the cause of the negative voltage spike but they were unable to prove the point experimentally because of the integrating effect of the conducting liner on fast signals.

Clearly there are many common features in the models inferred by the two groups. Both of them (and several other groups) see a growth of m = 2 and m = 1, coupling between the two modes and a sudden drop in the temperature of the interior following some postulated ergodisation of the field lines. For the Pulsator group that is effectively the end while for the T4 group it is merely the prelude with j(r) uniform for the further and explosive growth of the m = 2 instability. In both cases everything depends on the 'conventional' interpretation of the soft X-ray and external coil signals. Much more information will be needed to establish the details of the disruptive instability which may well differ from machine to machine and according to the mode of excitation. The main theoretical problem would seem to be to understand island formation and field-line ergodisation in a finitely conducting plasma.

If we now consider discharges well away from disruption then a general picture of the tokamak discharge (far from proven and certainly not universal) is of a central core dominated by m = 1 fluctuations and m = 0 relaxations inferred from soft X-ray emission, an outer region where recycling, impurity radiation and charge exchange predominate, and an intermediate region where the density and temperature gradients are maximum, where the main containment occurs but where we know that the electron containment is not classical (of which more later). Theoretically this is the region where drift waves would be expected to be unstable. Thus there is considerable interest in looking for density fluctuations in that region.

Measurements of density fluctuations by microwave scattering have been performed on ATC[25] and TFR[26] and by CO_2 laser light scattering on ATC. Fig.17 shows the 2 mm set-up used on TFR and Fig.18 the resultant measured frequency spectrum. By varying the angle between the lines of detection and of input a small range of k values in the meridional plane can be explored. The observed frequency spectrum is very broad and asymmetric. The asymmetry reverses above and below the equatorial plane and consequently can be interpreted as a Doppler effect due to plasma rotation. By absolute calibration the density fluctuations $\tilde{n}$ integrated over the observed k space ($4 - 5\ cm^{-1}$) are found to be $\tilde{n}/n_o \sim 3 \times 10^{-3}$.

Having measured the level of fluctuations and the frequency spectrum a major difficulty is to relate these to the plasma loss rate. The TFR group

assume that these fluctuations are due to the dissipative trapped electron mode and use the quasilinear theory to relate the electron thermal conductivity to the fluctuation level. They find the resulting conductivity $\sim 100 \div 200$ times too small to "explain" the observed transport. But the fluctuation measurements were limited by the geometry of the microwave system to regions of the plasma on the small major radius side of the column. If the fluctuation amplitude is greater on the outside then it might be possible to obtain consistency. In the ATC measurements it was found that the fluctuation level is larger by a factor of ~ 5 on the outside compared with the inside. The fluctuation level is estimated as $\tilde{n}/n_o \sim 10^{-2}$ on the inside and $\sim 5 \times 10^{-2}$ on the outside. The intensity of the turbulence is large even where the $\vec{k}$ vector makes large angles ($\sim 45^o$) with the poloidal direction. This is consistent with the general picture built up on both TFR and ATC of fluctuations isotropic in the meridional plane. Fluctuations in the same range of k have also been studied on ATC using small angle scattering of CO_2 laser light with homodyne detection. The results are in broad agreement with the microwave data showing $\tilde{n}/n_o \sim 3 \times 10^{-2}$ and the frequency spectra ~ 500 kHz wide. A major difference is that the CO_2 work showed a greater level of fluctuations on the inside (by 50%) than on the outside. But the CO_2 work was done with a different plasma, in particular with an aspect ratic of ~ 0.1 compared with ~ 0.2 for the microwave work. Using a simpler relation between fluctuations and transport the ATC group were able to show that the observed fluctuations could account for the observed loss rate.

A great deal more work of this kind will be needed to establish any clear correlation between density fluctuations, energy transport and instability theory. Measurements are needed with a wider range of wavelengths including far infra-red lasers, over a wider range of discharge parameters (and hence of confinement) and with better geometric access to permit full exploration of the scattering vector $\vec{k}$.

4. IMPURITIES, RECYCLING, PLASMA WALL INTERACTIONS

Tokamak reactor plasmas, apart from having a higher β, will also have to be a great deal cleaner than those in existing devices. For example, the presence of 1 tungsten ion in 500 electrons prevents ignition at any plasma temperature[27]. Present tokamak plasmas typically contain 1 - 10% of light impurities such as carbon and oxygen together with 0.1 - 1% of heavy metals such as iron, tungsten or molybdenum.

Present devices are commonly operated for pulse lengths of many particle

containment times, sometimes with only the initial gas filling and sometimes with auxiliary neutral gas injection. In the first case recycling at the walls is dominant and in the second as we shall see it is still important.

Fig.19 produced by the JET team illustrates the range of elementary processes at the wall. As we will see some of these processes are already known to have a profound effect on tokamak operation, the crudest example being that tokamak operation is itself only achievable after discharge cleaning has reduced the level of adsorbed gas on the wall. A full understanding will require much more detailed measurements of wall parameters and a major effort by surface physicists. A start has been made.

Early interest in impurities stemmed from the problem of explaining the difference between the conductivity temperature and the substantially higher measured electron temperature. Estimates of the impurity content in ST[28] based on spectroscopic measurements showed that the effective charge of the plasma $Z_{eff}(=\frac{\Sigma_z n_z Z^2}{n_e})$ plus the trapped particle effect was consistent with the idea of classical resistivity. It is now commonly accepted that

$$j_\phi(r) \propto \frac{T_e^{\frac{3}{2}}(r)E_o}{Z_{eff}(r)} \qquad ..(15)$$

where E_o is the mean toroidal electric field on the magnetic axis. It is usual to assume without proof that Z_{eff} is independent of r and hence to derive $j_\phi(r)$ and Z_{eff} from the measured profile of T_e and the known total current. There is little doubt that because of the high electron thermal conduction along field lines the electron temperature is constant on a magnetic surface. The assumption that the toroidal current is then given by the simple formula,

$$j_\phi = \text{const } T_e^{\frac{3}{2}} \cdot E \qquad ..(16)$$

is clearly wrong since we know from the Grad-Shafranov equilibrium equation that

$$j_\phi = \frac{A}{R} + BR \qquad ..(17)$$

ie inconsistent with (16) whether we take E to be independent of R or, consistent with a steady state, $E \propto 1/R$. The essential point is that convective motion of the plasma should be included in the Ohms Law. Nevertheless the simple form is probably adequate for present low β_θ high aspect ratio systems. The use of the trapped particle correction can also be objected to on the grounds that it is a subtle consequence of classical theory and since the radial

particle flux is orders of magnitude different from the classical value we have little basis for expecting the trapped particle effect.

The impurity influx into the system is typically determined by measuring the intensity of lines from relatively lightly stripped ions such as OII, CIII and FeII. This is because, in the outer layers the time for ionisation to state Z is short compared with the confinement time so that there is a relation between the line intensity and the source term of the form

$$\left(\frac{dn_e}{dt}\right)_{I^o} = \frac{2\pi}{\Delta r} \cdot Z \frac{S_{Z-1}}{Q_{Z-1}} B \qquad ..(18)$$

where $\left(\frac{dn_e}{dt}\right)_{I^o}$ is the electron density source term coming from the ionisation of the impurity I from its neutral state to charge Z, S and Q are the coefficients of ionisation and of excitation of state Z-1, Δr is the thickness of the radial zone from which the spectral line from state (Z-1) comes with intensity B ($ph.s^{-1}cm^{-2}sr^{-1}$). Measurements on TFR[29] for example showed a very high oxygen injection into a peripheral zone a few cms thick. Taking the measured Z_{eff} (from resistivity) in the central region of 6, corresponding to an oxygen concentration there of 9%, together with the particle confinement time for the centre (deduced from H_α measurements), required an influx of oxygen at the rate of 2×10^{13} cm^{-3} s^{-1}. The flux entering at the periphery deduced as above was $5 \times 10^{15} cm^{-3}$ s^{-1}. Thus it was concluded that only a small fraction of the injected oxygen reaches the centre of the discharge, the major part returns to the wall.

Earlier work on T4[30] in which the impurity content of the plasma was measured by the soft X-ray technique using foils showed a continuous <u>increase</u> in the "X-ray target" on axis in a "completely stable" high q discharge. This was interpreted as due to the classical concentration of high Z atoms predicted for example by Braginski and most simply understood as due to the radial electric field in the discharge. This field produces a force Z times greater on the impurity ions than on the protons so that in an <u>isothermal plasma</u> one expects

$$\frac{n_Z(r)}{n_Z(0)} = \left\{\frac{n_p(r)}{n_p(0)}\right\}^Z \qquad ..(19)$$

i.e., an intense concentration of impurity atoms near the discharge centre. This result was the cause of great gloom at the Culham Fusion Reactor Workshop

in 1975 where it was thought that this property of toroidal systems, namely the containment of impurities for longer than the protons (or even for ever) would limit such systems to short pulse and probably uneconomic operation. Since then both the theoretical and experimental positions have become confused and perhaps more hopeful. First the neo-classical version of the Braginski theory has been found to be extremely complex, and is complicated still further by the inclusion of temperature gradients and second it has been shown in many experiments including ST and TFR that impurities do not accumulate continuously in the centre of those discharges. The latest evidence comes from T10 where Z_{eff} remains low ($1 \div 2$) throughout the pulse, although the calculated injection of heavy metals by sputtering from the observed fast neutral flux at the wall would lead to a rise in Z_{eff} through the pulse by a factor 3.

The only direct method of measuring the central impurity concentration species by species is by observation of spectral line intensities from partially stripped impurities. The relevant lines are in the grazing incidence region where absolute calibration is difficult. However, even when the intensity is known, to obtain the concentration it is necessary to rely on a theoretical model relating the emission to the concentration. These models which for example calculate the distribution of charge states by balancing ionisation against recombination suffer from uncertainties regarding the cross-sections and have fluctuated in their conclusions in the recent past in a way which does not inspire confidence. Nevertheless concentration figures are produced by this method which it is claimed are accurate within a factor 2. An example is the result from studies of a particular DITE discharge which gave the principal impurities as Fe($\sim$0.004 n_e), Cr($\sim$0.002 n_e), Mo($\sim$0.002 n_e) and O($\sim$0.01 n_e) with the heavy metals accounting for $\sim$ 97% of the radiated power and 76% of the mean ion charge excess, $Z_{eff} - 1$.

The origin of the metal impurites in DITE has been the subject of a special study.[35] From the metallic deposit on optical windows (and all over the torus surface) it is concluded that $\sim 3 \times 10^{18}$ atoms are removed from the wall on each discharge corresponding to an effective removal rate of 0.04 atoms/ion compared with the sputtering coefficient for 200 eV H^+ ions on stainless steel of $\sim 10^{-4}$ atoms/ion. The composition of the deposited film is mainly stainless steel with about 10% of molybdenum from the limiter. Carbon probes which are subsequently analysed using Rutherford back-scattering of 3.5 MeV $^{14}N^+$ ions have been used to measure the concentration of impurity ions at various radii near the wall as a function of time. Figs.20 and 21 show the

results. The measured concentration increases with distance from the wall as impurity atoms entering the plasma become ionised and follow field lines until they intersect the probe. From the time dependent measurements it is found that the impurity influx is roughly proportional to plasma current and density. These results are again inconsistent with either sputtering or evaporation since in both cases the highest metal flux would be expected at the beginning and end of the pulse when the particle and energy fluxes to the wall are high. The DITE workers believe that the results are consistent with the evaporation due to the type of unipolar arcs first observed on pinches. Arc tracks have been directly observed by subsequent microscopic study of polished molybdenum probes inserted into the discharge. The introduction of hydrogen via a fast gas valve during a discharge results in an immediate reduction in the flux of iron atoms. Similar effects were observed with hydrogen in Pulsator and with oxygen in TFR and ST. This suggests that the introduction of cold gas at the edge lowers the electron temperature there and hence reduces arcing. This DITE work is with a relatively low ion temperature ($\sim$ 200 eV) and we would expect sputtering to become an important mechanism as the ion temperature rises above 1 - 2 keV if the wall cannot be protected in some way from ions and fast neutrals. Indeed in high power neutral injection work on TFR where the ion temperature was raised from 1200 to 1600 eV the intensity of the Mo XXXI line rose sharply by a factor approximately 2 during injection.

Recycling studies have been made on DITE[35] using a scanning Fabry-Perot interferometer to monitor the H_α and D_α lines for a series of discharges in deuterium following many in hydrogen. The results are shown in Figs.22 and 23. They show that deuterium which is ionised at the beginning of the discharge is rapidly lost and replaced by hydrogen. The results can be interpreted in terms of a quantitative model the principal features of which are the straight reflection of 60% of the neutral atoms striking the wall and the desorption from the metal surface of slow (< 10 eV) neutral hydrogen, this hydrogen being replaced by diffusion from the interior of the metal in the interval between pulses. The hydrogen in the bulk material is presumed to have been deposited there by inward diffusion during prolonged running in hydrogen. Note that at incident energies less than 1 keV the reflected neutrals will have energies close to their incident values and will have a high probability of penetrating to the centre of the discharge.

The tokamak wall problem is really the following: if the plasma near the edge of the discharge is cool there will be a lower influx of heavy metals but the channel will tend to contract due to the $j \propto T_e^{\frac{3}{2}}$ law so that q at the

edge of the plasma is reduced and the plasma disrupts. If the temperature at the edge is high the plasma does not disrupt but fills itself with heavy impurities. One solution which may be feasible in large machines ($\overline{na}$ is the important measure of large) such as JET is to have a cool boundary thick enough to screen the wall from charge exchange neutrals from the interior but nevertheless thin compared with the plasma radius. Another solution is to use a divertor in which escaping plasma is channelled magnetically into a chamber separate from the main torus in which high speed pumping is used in an attempt to remove impurities released by the plasma-divertor target interaction. A magnetic divertor operating on the toroidal field was used successfully in the Model C Stellarator. With its in principle axisymmetry a divertor operating on the poloidal field is more appealing both because it preserves the axisymmetry and because it is only necessary to modify the much weaker poloidal field. This type of divertor is to be investigated on two large tokamaks, ASDEX at Garching and PDX at Princeton, due to come into operation in the next year or two. At Culham we have been trying out on a small scale a third type of divertor, the so-called bundle type in which a localised bundle of flux lines is extracted from the torus by a pair of auxiliary coils[35].

Fig.24 shows examples of the three divertor types discussed above. A major practical advantage of the bundle type is that when it is turned off the full aperture of the torus is available for the discharge, whereas in the poloidal type a large fraction of the volume inside the toroidal field coils is devoted to the rings, baffles, getter pumps, etc of the divertor. A disadvantage of the bundle divertor is the total lack of symmetry with the toroidal field modulated at $\sim 2 \div 5\%$ on the magnetic axis and 100% on the separatrix surface. There are also very large magnetic forces on the bundle divertor coils and the current density has to be high to avoid interception of the escaping flux lines and plasma by the coils themselves. Thus it is that the first experimental bundle divertor that has been working on DITE for the last year or so is limited to operation at 10 kG toroidal field strength and hence to discharge currents of the order 50 kA.

The topology of the bundle divertor prevents fields from forming perfectly closed magnetic surfaces. Computations show that a field line experiences a small radial step each time it passes through the divertor. Although this breaks up the magnetic surfaces in the scrape-off region outside the separatrix, particles following these lines are trapped by the divertor target and so do not experience the radial step.

Three basic functions of the divertor have been clearly demonstrated while at the same time the confinement of the plasma inside the separatrix remained unaffected. The first function is that of plasma diversion; this is observed by cine-photography, mass spectrometry and infra-red scans of the temperature rise of the target. The plasma flow pattern confirms the computed shape of the diverted flux bundle. The plasma density at the wall of the torus measured by a Langmuir probe falls by a factor 5 and the torus wall recycling as measured by H_α emission is reduced. The second function of power diversion is demonstrated by the observation that approximately 60% of the ohmic power input is deposited on the divertor target whereas without the divertor most of the input power reached the wall in the form of radiation. Thirdly, the screening action by which the central plasma is shielded from gas emitted from the wall by the layer of diverted plasma is most readily demonstrated by pulsing in gas from the torus wall. Whereas the density of a non-diverted plasma can be raised by pulsing H_2 gas into the torus, it is difficult to raise the density of a diverted discharge in the same way (Fig.25). The effect of pulsing on the divertor half way through the discharge on various discharge parameters is shown in Figs.26 and 27. Note the substantial reduction in the OV line while the OII line representing injection is largely unchanged. This is due to the shielding action in which the ionised oxygen is lost along the field to the divertor before it can penetrate to the interior. Fig.27 shows the dramatic change in the radiated power profile coming from the reduction of heavy metals in the centre. An initial paradox was that despite all the evidence quoted the Z_{eff} was largely unchanged. First of all in these relatively low current cases Z_{eff} is in any case low at ~ 2. But the main point is that to maintain the same electron density in a diverted discharge it is necessary to pulse in much more H_2 gas than in the undiverted case. This leads to a higher recycling rate near the wall and in particular a higher injection rate of oxygen. This higher rate largely compensates the screening effect so that the oxygen content in the centre, which is primarily responsible for Z_{eff}, is the same in diverted and undiverted discharges. Clearly the very success of the divertor highlights the need for an internal refuelling method such as is provided by the injection of pellets or by very high power neutral injection. In addition we need to fit a bundle divertor capable of operating at the full toroidal field strength of DITE (28 kG) so that divertor experiments can be made with higher discharge currents and consequently in conjection with high power neutral injection. Note that the bundle-type of divertor has the advantage over a symmetric one of having a much thicker scrape-off layer of plasma to shield the main plasma from wall-emitted impurities. This is because in the

bundle type particles have to circle the torus round the major axis many times before entering the divertor chamber while in the poloidal type they need only circle the minor axis once. The thickness Δ of the scrape-off layer is related to the distance L along the lines and the perpendicular diffusion coefficient $D_\perp$ by the relation

$$\Delta = (D_\perp \frac{L}{c_s})^{\frac{1}{2}} \qquad ..(20)$$

where c_s is the plasma sound speed. For the particular DITE divertor $L \sim 10 \times 2\pi R$ and the observed thickness of the scrape-off layer of 7 cm is roughly consistent with $D_\perp \sim D_{BOHM}$. The screening function of the divertor may well turn out to be its most important one since even with 100% exhaust efficiency the wall will still be subjected to strong radiation and charge exchange fluxes.

5. TOKAMAK OPERATING REGIMES

It has long been known that the regimes of tokamak operation are limited. Too low a density leads to excessive runaways or to the so-called slide-away regime particularly well-documented on Alcator in which strong turbulence is excited by a relatively large ratio of the electron drift to random velocities. Too high a density leads to disruption and too low a q value of the limiter does the same. The density at which disruption begins has been shown by analysis of a large number of experiments (all with ohmic heating as the sole or dominant heating mechanism) to scale with the parameter B_ϕ/R. Now B_ϕ/R is a measure of the current density on the axis for $q = 1$ and since the loop voltaage and physical size of the experiments considered did not vary greatly, B_ϕ/R is roughly proportional to the ohmic power input. But it has long been known that B_ϕ/R and q are not the only parameters determining the operating regime. The discharge cleanliness is also an important parameter. This has recently been strikingly demonstrated on DITE by gettering 30 - 40% of the torus wall with titanium[35]. The getter source is evaporated continuously between discharges (10 - 20 minutes) and withdrawn from the torus $\sim$ 30 s before the shot. The evaporation rate of 2×10^{-2} g per discharge is sufficient to pump several times more gas than that introduced. With the wall gettered the density limit is considerably increased over the non-gettered by factors of 3 - 4, for a discharge of 150 kA and B_ϕ = 27 kG, a mean density of 7×10^{13} cm^{-3}, $\beta_\theta \simeq 0.6$, and $\tau_\epsilon \simeq 25$ ms is achieved. The results from these and other experiments are shown plotted in a normalised way $1/q$ vs $\frac{n_e R}{B_\phi}$ in Fig.28.

The high density limits with and without gettering are shown by the two curves. Gettering the DITE torus clearly extends its operating range into the same region in normalised parameter space as Alcator and Pulsator. How did Alcator and Pulsator achieve their performance without gettering? I do not know. It may be that particularly in the Alcator case the high power loading on the wall leads to exceptional cleanliness. It may be that both machines are effectively gettered by sputtered material from the limiter. In the DITE case the main effect of gettering is to reduce the influx of oxygen from the walls as gas is pulsed into the system. Oscillograms of the current, loop voltage (which gettering reduces by a factor 2) and mean electron density are shown in Fig.29. Also plotted are β_θ and τ_ε calculated from the change in diamagnetic flux and the measured power input. Although the hydrogen gas influx is constant between 0 and 180 ms, the density rise is interrupted by one or more pauses (Fig.30) lasting 10 - 30 ms when there is increased m.h.d activity and an increase in internal inductance. These are interpreted by the DITE group as major rearrangements of the discharge. A uniform density rise can be maintained through these m.h.d. periods by temporarily increasing the gas influx but the m.h.d. activity is unchanged. These observations may bear on the theoretical problem of explaining why the density rises continuously in Alcator and Pulsator with very little or no sign of a hollow density profile even though the penetration of neutrals to the centre would be expected to be small and indeed the lack of escaping fast neutrals from the centre at high $(\overline{na})$ shows it to be small.

In DITE the gettering reduces but does not eliminate the oxygen influx. During an early stage of the gettered discharge when the density is comparable to an ungettered case the intensity of the OV line (2718A°) is down by a factor ~9. There are bursts of increased oxygen influx during the density pauses (Fig.30) and it is supposed that with ungettered walls these would be larger and would cause disruption and a lower density limit. Even in the gettered case the higher density limit is still set by disruption preceded by a sharp rise in oxygen influx. Were this eliminated by some means there seems no reason why the density limit could not be increased further until ionisation of incoming hydrogen etc., produced an edge cooling sufficient to cause disruption.

The DITE observations and those on other machines are consistent with the model of disruption in which ohmic heating is insufficient to prevent cooling of the plasma edge; this leads to contraction of the column, a lowering of q at the boundary and a steepening in the radial gradient of current density leading eventually to m.h.d. instability and disruption. It must be remarked, however,

that I have yet to see clear definitive experimental evidence of this contraction occurring as the maximum density is approached.

According to this picture we would expect to see the critical density increase when ohmic heating is supplemented by auxiliary power. Experiments on ORMAK have indeed shown this, and hints of the effect have been seen on DITE. A large change should occur in the experiments shortly to be made in which the auxiliary power is much larger than the ohmic input.

In the DITE work, as on earlier machines, notably Alcator and before that T3, we see that as the density is increased so the energy containment time rises ($\tau_\varepsilon \propto n$) while at the same time the electron temperature falls only slightly.

6. ENERGY BALANCE

We consider here the energy balance of ohmically heated discharges. For the regime where the density is less than the critical value and in which strong neutral gas injection is not used detailed power balance studies have been made on several machines. The results show two basic types of discharges - "Dirty" ones in which the light impurity (oxygen and/or carbon) contamination is high, Z_{eff} is 3 - 10, the injection rate of heavy impurities is low, the radiation loss occurs predominantly in the outer regions and the electron temperature in the centre is high; "Clean" discharges with much lower light impurity contamination, the same Z_{eff}, high injection rate of heavy impurities, radiation loss dominant in central hot region and electron temperature there relatively low. These two operating modes were first clearly demonstrated on the ST machine. Here we quote as examples results from TFR ("Dirty") and DITE ("Clean").

On TFR[26] a detailed study was made of a discharge with $I \sim 290$ kA, $B_\phi = 54$ kG, $\bar{n} = 4.5\ 10^{13}$ cm^{-3}, $T_e(0) = 1.8$ keV, $Z_{eff} \sim 3$, $q(0) = 0.8$, $q(a) = 3.75$, and $\tau_\varepsilon = 17$ ms. For the discharge as a whole the measured power balance is as shown in the following table

ELECTRONS				IONS	
P_{ei}	$P_{RADIATED}$		P_e conducted	P_i cx charge exchange	P_i COND Conduction
	Bolometer	Spectra			
0.13 P_Ω	0.63 P_Ω	0.4 P_Ω+?	0.24 P_Ω	0.7 P_{ei}	0.3 P_{ei}

where P_Ω is the ohmic input. Evidently 63% of the input is radiated. The figure for radiation loss obtained from spectra is confined to studies in the wavelength range 100 - 1300 Å; presumably the extra loss required to agree with the bolometer measurement occurs at shorter wavelengths. The charge exchange loss is deduced from the measured flux of fast neutrals at the wall. The electron and ion conduction losses are obtained by subtraction and the energy exchange between ions and electrons is assumed to be classical.

From measurements of the density and temperature profiles, from the neutral density profile (from H_α) and from chordal bolometer measurements it is possible to construct the radial profiles of the power from within a volume limited by r. Fig.31 shows this profile. Note that the fraction of power radiated rises rapidly towards the wall indicating the preponderance of power radiated from the outer regions. Fig.32 shows the power lost by conduction and convection inside a volume limited by radius r obtained by subtraction from the curves of Fig.31. Also shown is the power loss given by a neo-classical calculation taking into account the measured parameters. Note that the actual loss is $\sim 10^2$ larger than the neo-classical theory predicts.

As an example of the "clean" or metal dominated discharge, I show DITE results[35]. During the period of operation of DITE ($\sim$ 1 year) the central electron temperature showed a slow but steady reduction and more recently persistently hollow temperature profiles with $T_{eo} \sim 200$ eV have been observed occasionally at first and then regularly and reproducibly as shown in Fig.33. Similar profiles have been observed in Ormak and more recently in PLT. The radiated power is measured with a thermopile mounted behind a collimator with a spatial resolution of 25 mm which can be scanned across the discharge diameter. It shows a large central peak and little indication of the peripheral radiating layer typical of oxygen dominated discharges in TFR. In the centre of the discharge the radiated power exceeds the ohmic input, calculated assuming $j \propto T^{\frac{3}{2}}$, by 70%. This excess of radiated power, mainly line radiation from metallic impurities, explains why these hollow profiles persist. But note that a peaked temperature profile would also persist because the ohmic input increases like $T_e^{\frac{3}{2}}$ whereas the radiated power varies like $T_e^{\,0}$ or $T_e^{\,-1}$. An intermediate state of power balance also exists but is unstable. The existing of the two stable states explains why the transition from hollow to peaked profile or vice versa can be brought about by quite small changes in the discharge conditions. In fact the hollow profile can be removed by exposing the vacuum system to air for a short time or by injecting helium. TABLE 5 shows the main parameters of the three discharge types. Note the

striking changes in central electron temperature. Fig.34 shows the profiles of ohmic power input and power radiated for the three cases. In the contaminated and neon cases we see the radiated power exceeding the ohmic input in the outer regions. A point of some theoretical interest is the q-profile for the hollow temperature case; this is shown in Fig.33 and is of course based on the assumption $j \propto T^{\frac{3}{2}}$; q is multi-valued versus radius while the observed m.h.d. activity (with external coils) is low. The general conclusion from this work is that the internal behaviour of the tokamak plasma is very much dependent on the state of the wall.

It is clear that if we are to understand the plasma physics of tokamaks, and in particular the anomalous electron conduction loss, then we must make sufficiently detailed measurements to enable the purely plasma physical phenomena to be separated from atomic physics such as line radiation and charge exchange. Moreover we must do this over a wide range of parameters in order to build up a data bank to compare with detailed theories or with general scaling arguments such as those advanced by Connor and Taylor. We saw one example of the type of measurement needed in the TFR case where the electron conduction versus radius was deduced for one discharge and compared with neo-classical theory. Another example taken from Ormak is shown in Fig.35. The electron thermal conductivity is deduced from measurements with many discharges using the relation

$$\chi_e \sim \frac{a^2}{4\tau_E} \qquad ..(21)$$

The results are presented as a function of the single parameter $(\nu^*)_{MIN}$ which is the minimum (versus r) ratio of the effective electron collision frequency to the bounce frequency. Again as on TFR the magnitude of χ_e ~10^2 larger than the neoclassical theory and agrees relatively well with a particular theoretical prediction for the non-linear dissipative trapped electron mode (shown dashed in Fig.35).

There appear to be no measurements which explicitly demonstrate what is frequently deduced from the fact that $\tau_E \propto n$, namely that $\chi \propto 1/n$. It can be argued that in the upper range of Alcator results, where Z_{eff} is said to be indistinguishable from unity, radiation losses cannot play any significant role. Nevertheless it would be nice to have experimental confirmation of this. A more general anxiety concerns that the fact that the electron conduction loss must be deduced by subtraction of radiation from ohmic input and with the limited accuracy of radiation loss measurements the error could be large unless the radiation loss is very small.

7. AUXILIARY HEATING

It has long been recognised that since the ohmic heating power input varies

like $T_e^{-\frac{3}{2}}$, and therefore falls off at high temperatures, some auxiliary heating method is required to take the plasma to higher temperatures and eventually to ignition. Transient heating of tokamak plasma by adiabatic compression in 2 and 3 dimensions has been successfully demonstrated on the ATC[34], TOSCA[32] and TUMAN[33] experiments. Apart from its transient nature this method suffers through the inefficient use of the volume inside the toroidal field coils. A very wide range of RF methods has been suggested and some have been tried. As mentioned in the section on equilibrium both magnetoacoustic wave and electron cyclotron resonance heating have been used to increase the value of β in low current Russian tokamaks. Other RF experiments such as those with lower-hybrid heating although interesting are still in a primitive stage and have only just begun to produce an impact on tokamak physics as such.

By contrast, neutral injection heating has been outstandingly successful. Injection powers in the range 200 - 500 kW have been used on the DITE, ORMAK, and TFR machines. This is to be compared with the ohmic input power of 0.5 - 1.0 MW in these same machines. The injection energy is typically $\sim$ 30 keV and the injection pulse length $\sim$ 40 ms. In early work with tangential injection it was shown on CLEO, ATC and ORMAK that the slowing down of fast injected ions is entirely classical. Thus the spectra of tangential, high energy charge exchange neutrals are in agreement with theoretical expectation. Fig. 36 shows such a spectrum taken with 200 kW of injection power into DITE. Fig. 37 shows for the same case the spectrum of lower energy charge exchange neutrals measured radially and indicating the increase in ion temperature from 340 to 610 eV. In this particular case the temperatures were also confirmed with a Fabry-Perot scanning interferometer monitoring the Doppler width of H_α.

The power flow with neutral injection is shown schematically in Fig.38. A fraction α of the power injected into the torus is lost by charge exchange of the fast ions and because some fast ions are born on orbits with drift surfaces which intersect the limiter. These losses tend to get rapidly worse for lower discharge currents because the neutral density inside the discharge is higher (lower particle containment) and because with lower poloidal field drift surfaces are more displaced from magnetic surfaces. As the trapped fast ions slow down they first give their energy predominantly to the electrons, slowing down by frictional drag, then as their energy falls so the coulomb cross-section for interaction with the background ions rises until for energies less than ϵ_{crit} the interaction is then mainly with the ions;

$$\epsilon_{crit} \sim \left(\frac{M}{m}\right)^{\frac{1}{3}} T_e \qquad ..(22)$$

so that the proportion of injection power $(\frac{\epsilon_{crit}}{\epsilon_{INJ}}) = (1-f)$ going to the ions increases with the mean electron temperature. In all present published experiments the injection power going to the ions is comparable with or greater than the power normally transferred to them from the electrons - i.e., there is a substantial change in the ion energy balance. In contrast, so far, the ratio

$$\frac{f(1-\alpha)P_{INJ}}{P_\Omega}$$

between the injection power and the ohmic power to the electrons has always been small. That is the electron energy balance is perturbed rather than changed.

In ORMAK[23] with 360 kW of tangential injection the central ion temperature is increased from 650 eV to 1830 eV (Fig.39). The temperature rise is confirmed by the neutron emission from a deuterium plasma with H_0 injection. Figs. 40 and 41 show the corresponding density and electron and ion temperature profiles without and with injection. The ion temperature with injection is substantially greater than the electron temperature in the central region. Although the electron temperature profile develops a central hollow, presumably the consequence of the injection of metallic impurities, the rise in the central ion temperature is found to depend linearly on the total neutral injection power.

In the TFR[31] work the injection is near perpendicular to the circular axis of the torus (10° to the meridional plane). As a consequence rather more of the injected power is lost due to open orbit effects. Up to 650 kW has been injected and with the experimental parameters it is divided roughly equally between direct losses to the wall, the ions and the electrons (i.e. one third each). The electron temperature is unchanged within the experimental errors ($\sim$ 10%) by injection. The ion temperature is increased from 0.9 to 1.9 keV (Fig.42) (cf. central electron temperature approximately 2 keV). In the outer regions the ion temperature is again larger than the electron temperature. The increase in the ion temperature is also found to depend linearly on the total injection power. This of course implies simply that the ion energy containment time is constant and therefore independent of T_i. From a detailed study of the ion energy balance at the radius 12 cm where the losses due to charge exchange and convection are negligible and using the

relation

$$\chi_i = \frac{P_{ei} + P_{Ni}}{4.45 \times 10^{-15} ne\nabla T_i} \quad (cm^2.s^{-1}.W.cm^{-3}.eV) \qquad ..(23)$$

an experimental plot showing the variation of χ_i with collision frequency is obtained (Fig.43). This shows an approximately constant plateau value of χ_i 2 - 3 times greater than the neo-classical theory predicts and extending without reduction into the banana regime.

At this point it is relevant to recall that the ion temperature in a wide range of ohmic-heated tokamaks shows a remarkable agreement with a formula proposed by Artsimovich[1] and derived by balancing the energy flux to the ions from the electrons against ion thermal conduction using the form appropriate for the plateau regime of neo-classical diffusion. (i.e., $\chi_i \propto r/R^2 . T_i^{\frac{3}{2}}$). The formula is

$$T_i = \text{const } (I.B_\phi R^2 n_e)^{\frac{1}{3}} A_i^{\frac{1}{2}}$$

where A_i is the atomic weight of the ion. The TFR neutral injection results which showed $\chi_i \propto T_i^{\,o}$ and in which the plateau value is maintained into the banana regime throws some doubt on the underlying basis of the Artsimovich formula. The apparent success of the Artsimovich formula and the observed classical behaviour of injected ions had given rise to the pleasing general conclusion that ion behaviour in tokamaks might be classical although the particle confinement, which clearly must involve the ions, is known to be non-classical. The general result from the injection experiments on DITE, TFR and ORMAK is that the ion energy containment time remained constant when the ions were heated.

Something of an enigma in both TFR and ORMAK is that the electron temperature remains unchanged or even falls although there is a sizeable additional input to them ($\sim$ 20 — 30% P_Ω) coupled with a reversal of the electron-ion energy flow. However in recent neutral injection experiments on DITE (and I believe on ORMAK) the electron energy content per unit length is observed to increase and moreover to increase linearly with the input power, i.e. again corresponding to an electron energy containment time that remains constant. These results are shown in Figs.44, 45 and 46. Note that these experiments were done with a gettered torus which reduces the ohmic input to $\sim$ 300 kW. The electron density is seen to be unchanged by injection and soft X-ray measurements show Z_{eff} also to remain unchanged and close to unity. Both the power into the electrons and the energy content per unit length are increased by approximately 25%. It may be that in the earlier TFR and ORMAK work the

heating effect of injection was compensated by an increased level of impurities. Certainly in the TFR case the Mo XXXI line increased by a factor 2. We note also that in both TFR and ORMAK the ion temperatures are increased to the level ($\sim$ 2 keV) where sputtering would be expected to be important while in the DITE case the ions are all the time much cooler.

8. OVERALL PICTURE

What is the overall picture of tokamak behaviour that we can construct from the experimental results? The following seem to me the main points:-

1. Tokamak operation is bounded by the disruptive instability at high density and at high current and by runaway phenomena at low current.
2. The disruptive instability is the consequence of m.h.d. instabilities, $m = 1$ on the axis when q there falls below 1, and $m = 2$ tearing modes near the boundary. After some growth of these modes there is a coupling between them and eventually a near explosive loss of plasma energy from the centre of the discharge, a flattening of the current profile and the expulsion of poloidal flux.
3. The disruption is caused at high density by cooling of the outer edges, contraction of the channel and hence a lowering of q.
4. Disruption at high current is simply due to the lowering of q.
5. By special measures, such as an unusually close-fitting conducting shell, or by current programming, discharges can be operated with $1 < q < 3$. But the resulting confinement is poor.
6. Surprisingly accurate empirical scaling laws for the energy confinement time can be constructed from the data for ohmic heated systems. These laws are demonstrably incompatible with the basic plasma physics equations. Therefore overall tokamak behaviour is inexplicable on the basis of plasma physics alone.
7. There are density fluctuations in the interior of tokamaks with some of the properties of drift waves. The role of these fluctuations in the confinement is not yet known.
8. The electron thermal conductivity across the field lines is typically 10^2 times the neo-classical value. From the gross confinement properties it is inferred that this anomalous loss falls as the density increases. But there is a lack of clear data showing this scaling after allowing for other losses such

as radiation, charge exchange, etc.

9. The particle containment is also anomalous. Indeed in some regions of the discharge the neo-classical theory would predict a radial influx of particles whereas in practice an outflow is always observed. The particle containment time is difficult to measure accurately in the discharge centre because of the problem of measurement of neutral density there. Most groups conclude that roughly τ_p = constant x τ_E where the constant ranges from $1 \div 10$ in different experiments.

10. The plasma resistivity parallel to the magnetic field is, within experimental error, classical in the normal operating tokamak range (i.e. not at low density). The difference between the 'conductivity temperature' and the actual electron temperature is accounted for by the presence of impurities.

11. The ion temperature in ohmic-heated systems shows remarkable agreement with the Artsimovich formula which was derived on the basis of neo-classical plateau ion thermal conductivity. However, recent experiments with neutral injection heating have indicated temperature and collision frequency variations of the conductivity incompatible with the neo-classical theory.

12. By auxiliary heating or by sudden reductions in current the poloidal beta has been transiently raised to approximately 7 without any loss of equilibrium or confinement.

13. For $q > 3$ tokamaks with and without conducting shells are indistinguishable in their confinement and stability properties.

14. Fast ions from neutral injection are observed to slow down classically in the tokamak plasma.

15. Wall processes play a vital role in determining the radiation losses from the system. These losses in turn influence the current profile and consequently the m.h.d. stability of the column.

9. FUTURE EXPERIMENTAL WORK

I summarise the work for the next ~ 5 years as follows:-

(i) Continuous development of better diagnostics. Notable problems at the moment are the measurement of ion temperature and the measurement of the poloidal magnetic field.

(ii) More extensive measurements on existing machines. The main need would seem to be to establish the parametric variation of

particular processes, primarily the cross-field electron thermal conduction, to enable a comparison with plasma theory to be made and an understanding developed.

(iii) Development of auxiliary heating techniques. Neutral injection is already established at the ~ 1 MW, 40 keV per unit level. But future large $\overline{na}$ machines will require higher injection energies ~ 100 keV and eventually perhaps 1 MeV. This promises to be extremely difficult. R.F. methods may eventually be better, in particular ECRH where 100 kW units have been developed in the Soviet Union, where the frequency is too high to affect confinement, and where we do not expect the magnetic field strength, and hence the frequency, to change much as we scale towards a reactor.

(iv) Application of intense neutral injection at present energy level to present scale devices to test beta limits, to test confinement scaling, to vary the current density profile, to test multicomponent tokamak schemes and to escape from the heating instability inherent in ohmic dominated systems (PLT, ASDEX, DITE, TFR 600).

(v) Testing of divertor concepts (ASDEX, PDX and full-field bundle divertor on DITE).

(vi) Testing of ultimate limits on ohmic heating in very high field, small physical size tokamaks (Frascati tokamak, Alcator C).

(vii) Construction and eventual testing of multi-megampere machines designed to obtain near ignition plasma conditions (T20, JET, TFTR and JT60).

Of these last machines only TFTR and JT60 are at present under construction.

10. THEORETICAL PROBLEMS

Outstanding theoretical problems are

(i) Understanding the disruptive instability. This is of paramount importance since it is this instability which limits the maximum current and plasma density. The problem is the non-linear evolution of hydromagnetic modes; in particular the growth of islands and field line ergodisation in a conducting plasma. Does the latter occur explosively? Will the disruptive instability go away at higher temperatures due to finite Larmor radius and other kinetic effects?

(ii) Understanding the cross-field thermal conduction. Is it due to residual hydromagnetic turbulence and consequent magnetic surface breakage, or electrostatic modes? If the latter why does it appear to vary like n_e^{-1}? Current driven drift waves? Supporting evidence from the Culham Levitron and the TORSO stellarator.

(iii) Understanding the particle diffusion. In particular the behaviour of impurities is of vital importance.

(iv) What are the equilibrium beta limits? Can they be maintained for more than a fraction of a field diffusion time?

These seem to me to be the big issues. There are in addition many other matters which are important if we are to make progress, e.g. the accurate calculation of radiation losses from impurities, computer modelling of the complete discharge behaviour etc.

The next five years promise to be as interesting as the last.

TABLE 1

REPRESENTATIVE TOKAMAKS

DEVICE	COUNTRY	R_o (cm)	a(cm)	B_ϕ (kG)	Ip (kA)	q	Air or Iron Core	Stabilising Shell Yes or No
T-3	USSR	100	17	25	100	4	Iron	Yes
T-4	USSR	100	17	50	200	4	Iron	Yes
ORMAK	USA	80	23	18	200	2.9	Iron	Yes
ST	USA	109	13	40	130	2.4	Iron	Yes
ATC	USA	88-35	17-11	20-50	80-200	4.1	Air	No
TFR	FRANCE	98	20	50	300	4.1	Iron	Yes
PULSATOR	FRG	70	12	28	80	3.6	Iron	Yes
ALCATOR	USA	54	9.5	75	100	6	Air	Yes
DITE	UK	112	23	28	200		Iron	No
PLT	USA	130	40	35(46)	600	3.6	Air	No
T-10	USSR	150	37	35(50)	400		Iron	Yes
DOUBLET IIA	USA	66	35x100	8	140	6.5	Air	No
TOSCA	UK	30	10		25		Air	No
JFT-2	JAPAN		25	18	150			Yes
DIVA	JAPAN				15		Iron	Yes
FT	ITALY	83	21	100	1000		Air	Yes
PDX	USA	140	45	50	500		Air?	No
ASDEX	FRG	154	40	30	500		Air	No
DOUBLET III	USA	140	45x150	26(42)	2500(5000)		Air	No
JET	EUROPE	296	125x210	27	2600		Iron	No
TFTR	USA	248	85	52	2500		Air	No
JT60	JAPAN	300	100	50	3000		Air	No
T-20	USSR	500	200	30	5000		Iron	Yes

TABLE 2. DATA FOR HYDROGEN PLASMAS

Machine [Reference]	R (m)	a (m)	I MA	U (V)	B_T (kG)	q_a	$\bar{n}_e$ (10^{13} cm^{-3})	T_{eo} (keV)	T_{io} (keV)	τ_E (ms)
T3[2]	1.00	0.15	0.028	-	26	10.4	2.0	-	-	1.2
T3[2]	1.00	0.15	0.030		17	6.4	2.0	-	-	1.6
T3[2]	1.00	0.15	0.042	-	17	4.6	2.0	-	-	1.4
T3[2]	1.00	0.15	0.043	-	26	6.8	2.0	-	-	2.0
T3[2]	1.00	0.15	0.055	-	26	5.3	2.0	-	-	2.5
T3[2]	1.00	0.15	0.060	-	26	4.9	2.0	-	-	4.0
T3[2]	1.00	0.15	0.065	-	26	4.5	2.0	-	-	4.2
T3[2]	1.00	0.15	0.070	-	26	4.2	2.0	-	-	2.3
T3[2]	1.00	0.15	0.066	-	34	5.8	2.0	-	-	3.8
T3[2]	1.00	0.15	0.080	-	34	4.8	2.0	-	-	5.6
T4[3]	1.00	0.17	0.110	3.5	25	3.3	1.0	2.25	-	3.9
T4[3]	1.00	0.17	0.110	3.5	25	3.3	2.0	1.55	-	6.7
T4[3]	1.00	0.17	0.110	3.5	25	3.3	3.0	1.42	-	9.2
ST[4]+	1.09	0.10	0.042	3.15	44	4.8	1.9	1.45	-	3.9
ST[4]+	1.09	0.12	0.039	2.5	27	4.0	2.2	0.87	0.30	4.3
ST[4]+	1.09	0.11	0.045	4.35	35	4.3	1.5	1.30	-	2.3
ST[4]+	1.09	0.06	0.010	3.7	27	4.5	0.8	0.45	-	0.59
ST[9]+	1.09	0.13	0.063	3.4	43	5.4	0.8	1.3	-	2.3
ST[8]+	1.09	0.13	0.066	2.3	37	4.3	2.0	2.2	-	10.4
ST[5]+	1.09	0.14	0.040	3.9	27	6.1	0.9	0.6	-	1.5
ST[6]	1.09	0.12	0.044	2.6	35	5.3	0.65	0.87	0.20	2.6
ST[7]+	1.09	0.13	0.100	2.3	37	2.9	2.4	2.10	0.50	7.5
CLEO[10]	0.90	0.17	0.072	4.0	16.5	3.7	2.1	-	0.20	4.0
CLEO[10]	0.90	0.17	0.050	4.0	13.9	4.5	1.6	-	-	2.5
CLEO[10]	0.90	0.12	0.034	3.5	20.0	4.7	1.0	-	-	1.9
CLEO[10]	0.90	0.18	0.034	3.1	20.0	10.6	1.0	-	-	1.9
CLEO[10]	0.90	0.17	0.068	3.6	20.0	4.7	2.4	-	0.20	2.9
CLEO[10]	0.90	0.17	0.058	3.6	20.0	5.5	1.7	-	-	2.7
ORM[11]	0.80	0.23	0.160	3.0	18	3.7	2.0	1.2	0.39	9.0
ORM[12]	0.80	0.23	0.095	2.5	18	6.3	1.25	0.68	0.22	3.1
ORM[12]	0.80	0.23	0.095	3.8	18	6.3	0.8	0.44	0.19	2.2
ORM[13]	0.80	0.23	0.125	3.0	19	5.0	2.1	1.05	0.39	5.5
PULS[14]	0.70	0.11	0.06	2.5	27	4.7	1.3	0.85	0.15	1.5
PULS[14]	0.70	0.11	0.06	2.5	27	4.7	7.0	0.75	0.3	6.5
PULS[14]	0.70	0.11	0.06	2.5	27	4.7	12.0	0.5	0.3	10.0

TABLE 2. DATA FOR HYDROGEN PLASMAS

(Continuation)

Machine [Reference]	R (m)	a (m)	I (MA)	U (V)	B_T (kG)	q_a	$(10^{13} \bar{n}_e\ cm^{-3})$	T_{eo} (keV)	T_{io} (keV)	τ_E (ms)
TFR[15]	0.98	0.20	0.19	3.2	50	5.3	2.0	2.5	0.76	8.1
TFR[15]	0.98	0.20	0.20	2.6	40	4.1	2.4	1.9	0.82	13.2
TFR[15]	0.98	0.20	0.30	3.2	50	3.4	3.7	2.04	0.97	11.4
TFR[16]	0.98	0.20	0.11	3.3	20	3.7	1.6	0.85	0.51	6.6
TFR[16]	0.98	0.20	0.17	2.8	40	4.7	2.2	1.79	0.65	7.6
TFR[16]	0.98	0.20	0.20	3.0	40	4.1	3.5	-	0.83	9.2
TFR[16]	0.98	0.17	0.14	2.8	42	4.5	1.5	1.57	0.52	6.0
ALC[17]	0.54	0.095	0.053	2.3	55	8.7	4.9	0.6	0.32	4.4
ALC[17]	0.54	0.095	0.082	2.6	45	4.6	19.0	0.57	-	12.8
ALC[18]	0.54	0.095	0.066	-	44	5.9	15.0	-	-	10.0
ALC[18]	0.54	0.095	0.100	-	75	6.3	40.0	0.8	0.8	20.0
ATC[19]	0.88	0.17	0.078	3.0	15	3.2	1.9	1.1	0.20	3.2
ATC[19]	0.88	0.17	0.076	2.5	15	3.2	0.6	0.95	0.12	0.65
ATC[19]	0.88	0.17	0.067	2.5	15	3.7	1.7	0.75	0.17	1.6
ATC[19]	0.88	0.17	0.078	2.4	15	3.2	2.1	0.70	0.20	2.1
ATC[19]	0.88	0.17	0.080	2.4	15	3.1	1.8	0.83	-	3.3
TOSCA[22]	0.30	0.08	0.020	-	7	3.7	2.0	-	-	0.5
				DEUTERIUM PLASMAS						
ALC[17]	0.54	0.095	0.040	2.4	40	8.4	5.2	0.65	-	6.2
ALC[17]	0.54	0.095	0.031	2.2	55	14.8	5.7	0.50	-	7.6
ALC[17]	0.54	0.095	0.044	3.0	50	9.5	9.7	0.57	-	7.9
TFR[20]	0.98	0.20	0.096	1.85	50	10.0	2.0	1.53	-	15.0
TFR[20]	0.98	0.20	0.145	1.85	50	7.0	2.3	2.1	0.65	19.5
TFR[20]	0.98	0.20	0.200	1.75	50	4.8	3.5	2.05	-	22.0
TFR[20]	0.98	0.20	0.303	1.88	50	3.3	4.7	2.21	-	22.7
TFR[16]	0.98	0.20	0.250	1.4	50	4.1	3.4	2.38	0.77	27.6
TFR[20]	0.98	0.20	0.140	2.7	25	3.6	2.9	1.15	0.55	14.5
TFR[20]	0.98	0.20	0.141	2.08	33	4.8	2.6	1.55	0.6	17.5
TFR[20]	0.98	0.20	0.134	1.85	40	6.0	2.5	1.8	0.63	20.5

+ For some cases only τ_{Ee} is quoted, in these cases we have multiplied by a factor 1.15 to allow for the contribution of the ions.

TABLE 2. ADDITIONAL DATA NOT USED IN SCALING

Machine [Reference]	R (m)	a (m)	I (MA)	U (V)	B_T (kG)	q_a	$\bar{n}_e$ (10^{13} cm^{-3})	T_{eo} (keV)	T_{io} (keV)	τ_E (ms)
HYDROGEN PLASMA										
PLT [24]	1.30	0.40	0.59	1.5	35	3.6	2.6	1.9	1.6	40
DEUTERIUM PLASMA										
T10 [25]	1.50	0.37	0.4	2.0	35	4.0	3.7	1.2	0.8	40

TABLE 3. RESULTS OF BEST FIT OF τ_E TO VARIOUS COMBINATIONS OF PARAMETERS

Trial Number	Constant Multiplier τ_E in ms	Exponents of independent variables and standard deviations								Correlation Coefficients
		R	a	R/a	B_T	I	n_e	A_i	T_{eo}	
Scaling 1										
1.	(2.7±0.9)		1.57±0.18		0.88±0.13		0.61±0.08	0.65±0.21		0.92
2.	15.4±3.5	0.97±0.24				0.69±0.08	0.70±0.08	1.10±0.18		0.93
	As 2 but selected for $q \approx 4$									
3.	17.8±4.8	0.98±0.24				0.71±0.09	0.65±0.09	0.96±0.23		0.96
4.	2.9±1.0		1.86±0.27	0.43±0.30	0.77±0.15		0.70±0.10	0.73±0.21		0.92
5.	2.3±0.8		1.84±0.29	0.18±0.31	0.99±0.15		0.68±0.11			0.91
Scaling 2										
6.	5.1±1.6		2.13±0.44	0.91±0.37	0.49±0.16		0.84±0.09	0.62±0.17	0.25±0.16	0.96
7.	3.9±1.4		2.30±0.50	0.85±0.42	0.72±0.17		0.86±0.10		0.20±0.19	0.94

TABLE 4 Comparative Predictions for τ_E and T_{eo} for given assumed conditions $\gamma_R Z_{eff} = 1$, $\bar{n}_e = 5$, $A_i = 2$, $\bar{n}_i T_{io} = \bar{n}_e T_{eo}$ and parabolic profiles.

			T-10	DITE	PLT	TFTR	JET (basic)
	a	(m)	0.37	0.27	0.45	0.85	1.25
	R	(m)	1.50	1.17	1.30	2.48	2.96
	B_T	(kG)	50	28	46	52	27.7
	$I(q_a = 4)$	(MA)	0.57	0.22	0.90	1.89	1.83
Scaling 1 Table 3 Line 1	τ_E	(ms)	74	27	94	280	300
	T_{eo}	(keV)	0.79	0.41	0.92	0.93	0.50
Scaling 2 Table 3 Line 6	τ_E	(ms)	85	29	93	400	480
	T_{eo}	(keV)	0.84	0.42	0.92	1.07	0.61

TABLE 5

	1 (hollow profile)	2 (air contaminated)	3 (2% Neon)
I_p (kA)	176	199	120
V (V)	4.7	3.3	3.3
B_T (T)	2.7	2.7	2.0
$\bar{n}_e (10^{19} m^{-3})$	1.7	2.1	1.6
Z_{eff}	6.3	6.6	6.3
T_{eo} (eV)	205	1100	940
β_{pe}	0.09	0.14	0.20

REFERENCES

1. ARTSIMOVICH, L.A. - Nuc.Fus.12 (1972) 215

2. FURTH H.P. - Nuc.Fus.15 (1975) 487

3. ARTSIMOVICH, L.A. ET AL - Proc. 3rd Conf. Plasma Physics and Controlled Nuclear Fusion Research, Novosibirsk, August 1968

4. PEACOCK, N.J. ET AL - Nature 224 (1969) 488 and CLM-R-107 (Culham Report with more detail)

5. MUKHOVATOV, V.S., SHAFRANOV, V.D. - Nuc.Fus.11 (1971) 605

6. JET Report R-5 (1975).

7. SHEFFIELD, J. - 'Plasma Scattering and Electro-magnetic Radiation', Academic Press, 1975

8. GORBUNOV, E.P., MIRNOV, S.V., STRELKOV, V.S. - Nuc.Fus.10 (1970) 43

9. DAUGHNEY, C.C. - Nuc.Fus.15 (1975) 967

10. HUGILL, J., SHEFFIELD, J. - Empirical Tokamak Scaling - submitted to Nuc.Fus.

11. CONNER, J., TAYLOR, J.B. - Scaling Laws for Plasma Confinement - to be published in Nuc.Fus.

12. IVANOV, N.V., KOVAN, I.A. - Proc. 5th Int.Conf. Plasma Physics and Controlled Nuclear Fusion Research, Tokyo 1974 CN-33/A9-5

13. ALIKAEV, V.V. ET AL - Proc. 5th Int.Conf. Plasma Physics and Controlled Nuclear Fusion Research, Tokyo 1974 CN-33/A9-4

14. APGAR, E. ET AL - Proc. 6th Int.Conf. Plasma Physics and Controlled Nuclear Fusion Research, Berchtesgaden 1976 CN-33/A5

15. MEISEL, D. ET AL - Proc. 6th Int.Conf. Plasma Physics and Controlled Nuclear Fusion Research, Berchtesgaden 1976 CN-35/A6

16. FREEMAN, R.L. ET AL - Proc. 6th Int.Conf. Plasma Physics and Controlled Nuclear Fusion Research, Berchtesgaden 1976 CN-35/PD-1

17. CALLEN, J.D. ET AL - Proc. 6th Int.Conf. Plasma Physics and Controlled Nuclear Fusion Research, Berchtesgaden 1976 CN-35/B10

18. MIRNOV, S.V. - Proc. 4th Int.Conf. Plasma Physics and Controlled Nuclear Fusion Research, Madison 1971 CN-28/F5

19. KARGER, F. - Proc. 6th Int.Conf. Plasma Physics and Controlled Nuclear Fusion Research, Berchtesgaden 1976 CN-35/A7

20. ARTSIMOVICH, L.A. ET AL - Proc. 4th Int.Conf. Plasma Physics and Controlled Nuclear Fusion Research, Madison 1971 CN-28/C8

21. VON GOELER, S. ET AL - Princeton MATT Report 1060 (1974)

22. ÉQUIPE, T.F.R. - Proc. 6th Int.Conf. Plasma Physics and Controlled Nuclear Fusion Research, Berchtesgaden 1976 CN-35/A8

23. BERRY, L.A. ET AL - Proc. 6th Int.Conf. Plasma Physics and Controlled Nuclear Fusion Research, Berchtesgaden 1976 CN-35/A4-1

24. MIRNOV, S.V. ET AL - Proc. 6th Int.Conf. Plasma Physics and Controlled Nuclear Fusion Research, Berchtesgaden 1976 CN-35/A9

25. GOLDSTON R.J. ET AL - Proc. 6th Int.Conf. Plasma Physics and Controlled Nuclear Fusion Research, Berchtesgaden 1976 CN-35/A11

26. ÉQUIPE, T.F.R. - Proc. 6th Int.Conf. Plasma Physics and Controlled Nuclear Fusion Research, Berchtesgaden 1976 CN-35/A3

27. MEADE, D. - Nuc.Fus.14 (1974) 289

28. DIMOCK, D. ET AL - Proc. 4th Int.Conf. Plasma Physics and Controlled Nuclear Fusion Research, Madison 1971 CN-28/C-9

29. ÉQUIPE, T.F.R. - Proc. 5th Int.Conf. Plasma Physics and Controlled Nuclear Fusion Research, Tokyo 1974 CN-33/A6-1

30. VERSHKOV, V.A., MIRNOV, S.V. - Nuc.Fus.14 (1974) 383

31. ÉQUIPE, T.F.R. - Proc. 6th Int.Conf. Plasma Physics and Controlled Nuclear Fusion Research, Berchtesgaden 1976 CN-35/A4-2

32. CIMA ET AL. - Proc. 6th Int.Conf. Plasma Physics and Controlled Nuclear Fusion Research, Berchtesgaden 1976 CN-35/A10-5

33. KAGANSKI, M.G. ET AL. - Proc. 6th Int. Conf. Plasma Physics and Controlled Nuclear Fusion Research, Berchtesgaden 1976 CN-35/A12

34. BOL, K. ET AL. - Proc. 5th Int.Conf. Plasma Physics and Controlled Nuclear Fusion Research, Tokyo 1974 CN-33/A4-2

35. PAUL, J. W. M. ET AL - "DITE Tokamak Presentations Eighth Conference on Controlled Fusion and Plasma Physics, Prague, September, 1977". Culham Preprints CLM-P492 and 493, 1977.

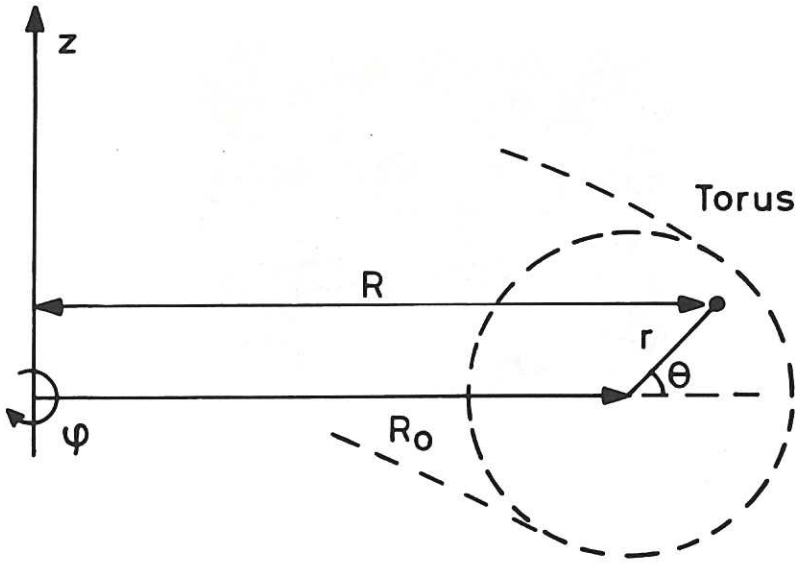

Fig.1 Co-ordinate system.

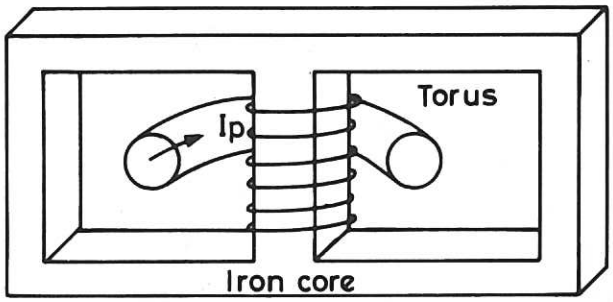

(a) General arrangment

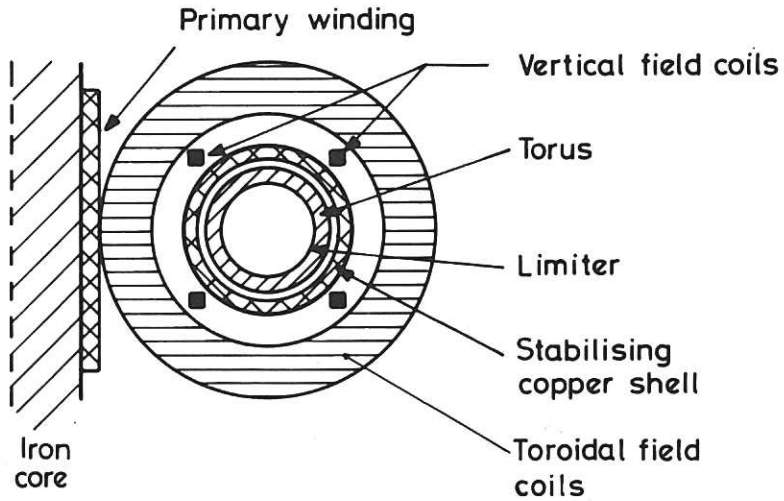

(b) Meridional cross-section

Fig.2 Standard Tokamak
(a) General arrangement
(b) Meridional cross-section.

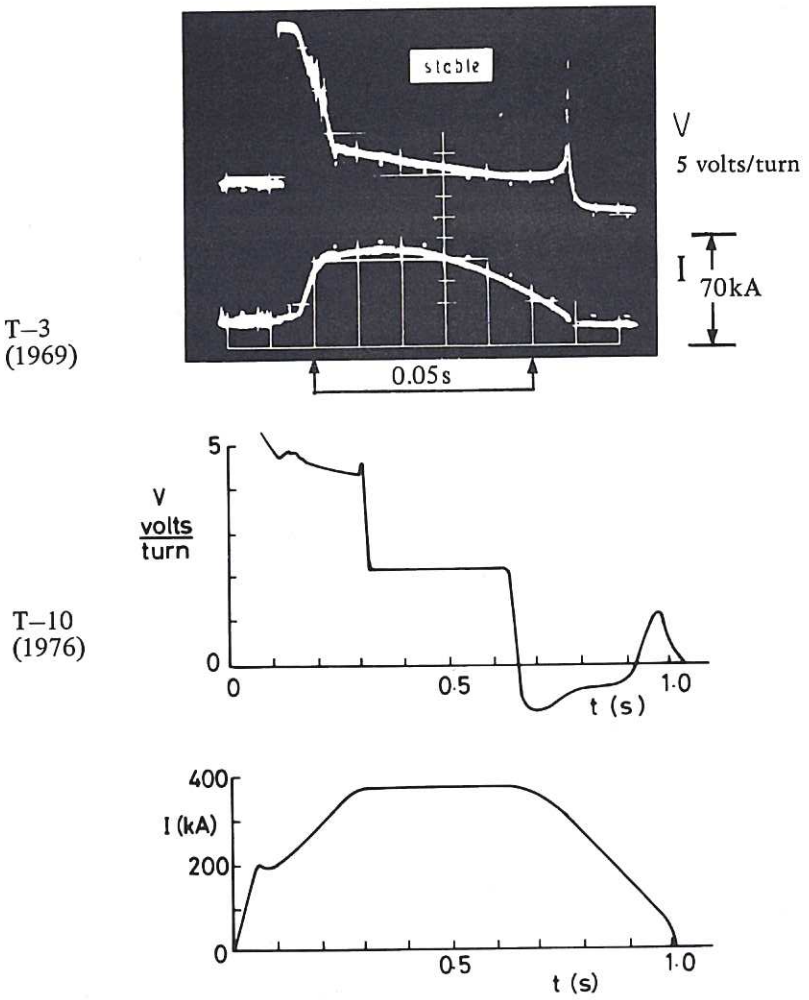

Fig.3 Current and voltage oscillograms for T-3 (1969) and T-10 (1976) discharges. Note substantial increases in current and pulse length with loop voltage relatively unchanged.

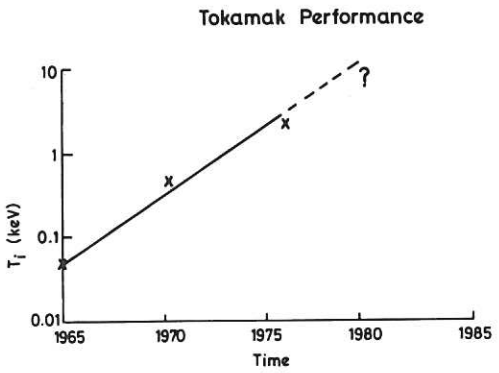

Fig.4 Tokamak performance.

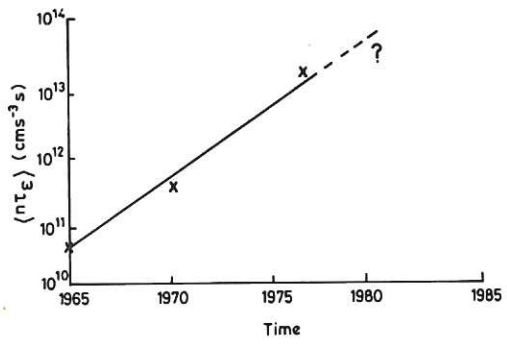

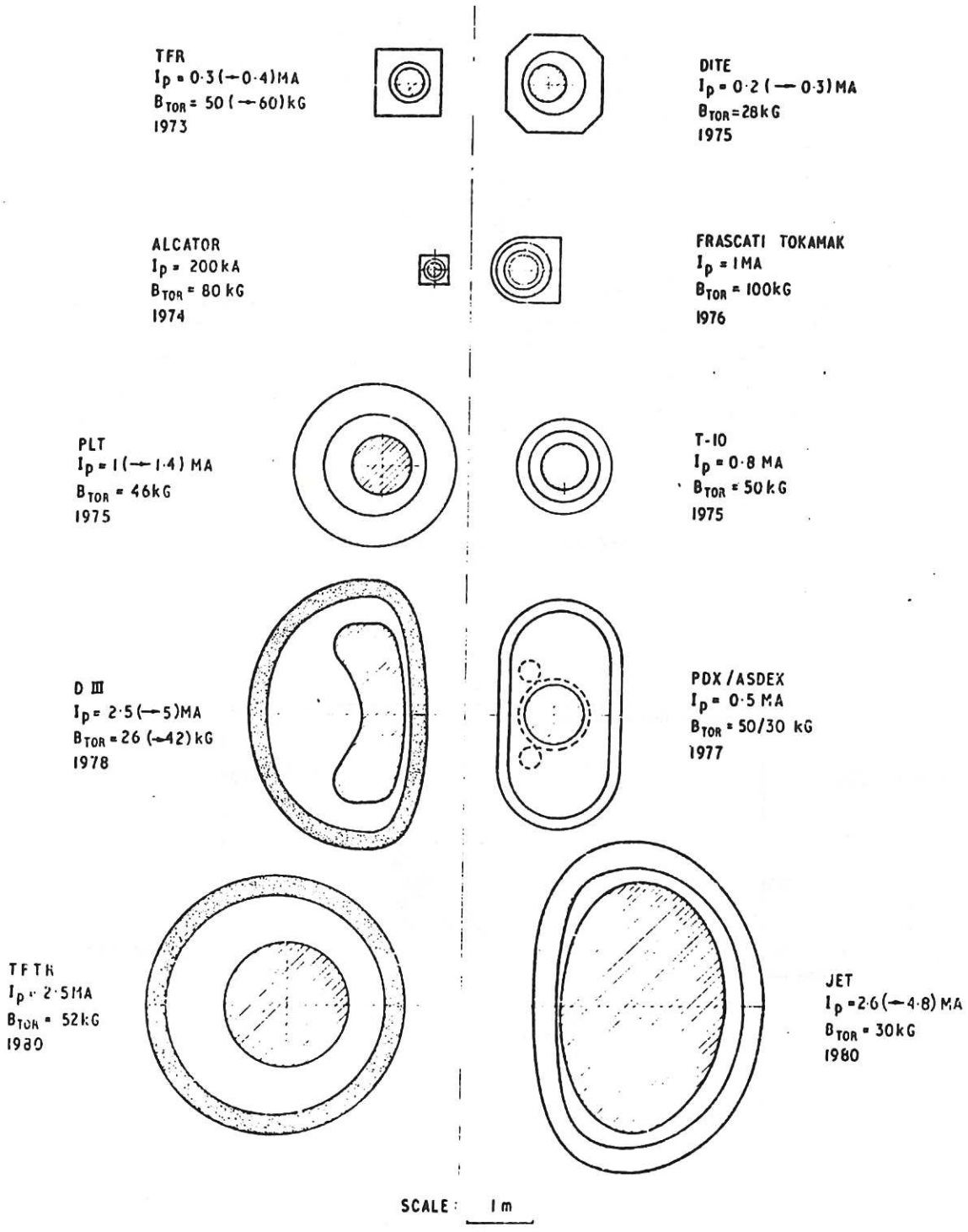

Fig.5 The relative size of the main devices which are at present in operation, under construction or in design throughout the world. Dimensions are to scale and the plasma current and magnetic field are given in each case.

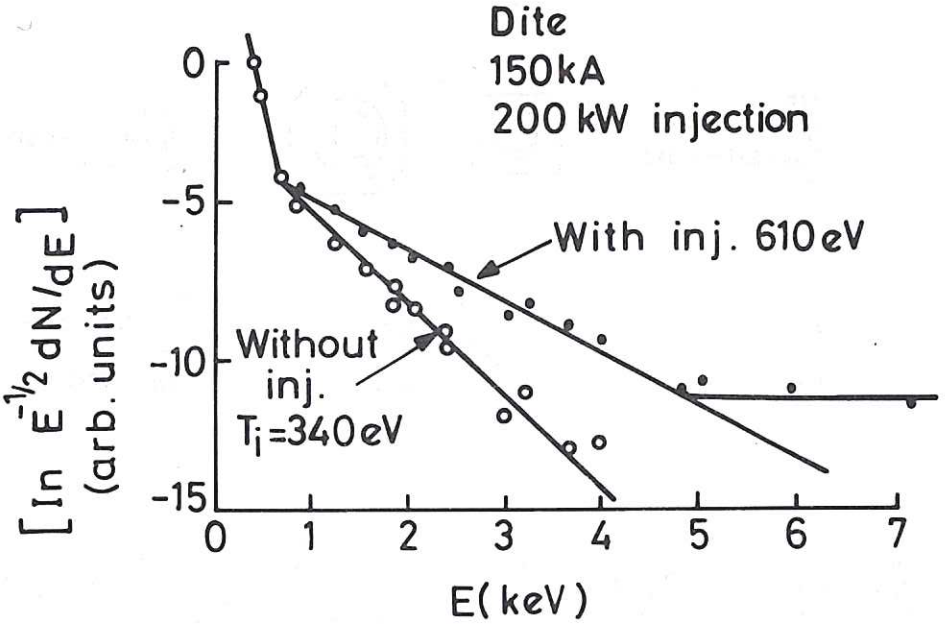

Fig.6 Charge exchange neutral spectrum.

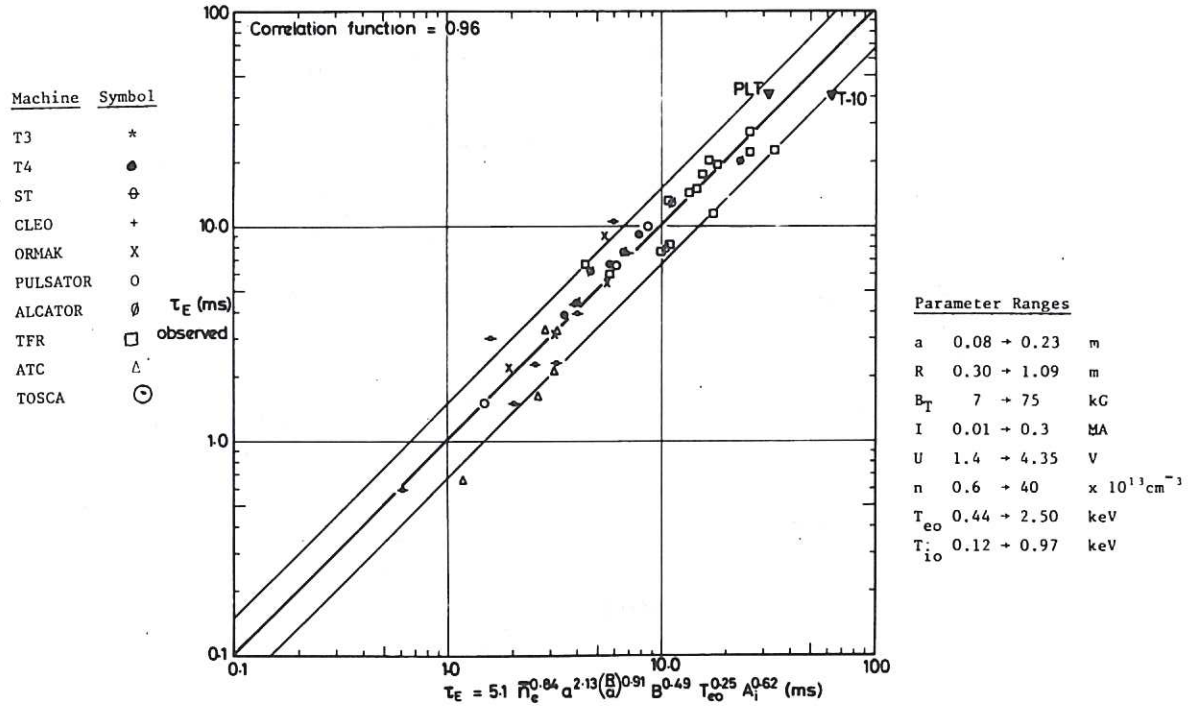

Fig.7 Machine symbol and parameter ranges.

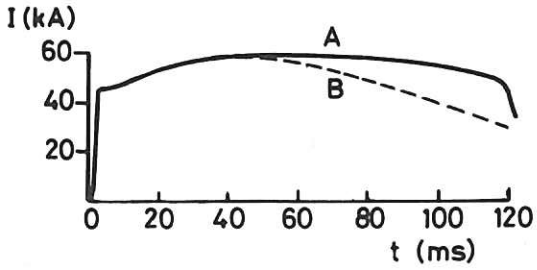

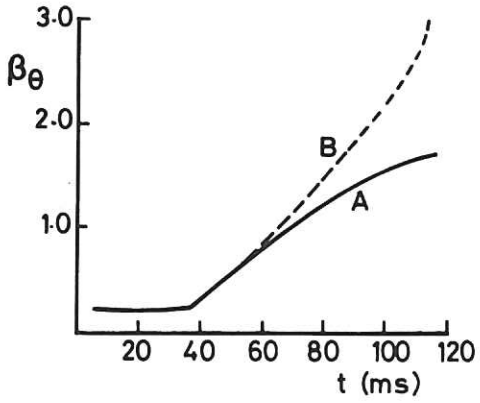

Fig.8 Pulsator – β_θ results.

Doublet II A results

	Doublet	Ellipse
B_ϕ (kG)	8·1	8·1
I_p (kA)	140	75
T_e (o) (eV)	350	350
n_e (o) (cm^{-3})	$3{\cdot}7.10^{13}$	$2{\cdot}9.10^{13}$
ε (elongation)	2·9	1·5
q (limiter)	6·5	2·6
q (o)	~ 1·2	≲ 1
β_ϕ (o) (%)	1·0	0·8

Fig.9 Doublet IIA results.

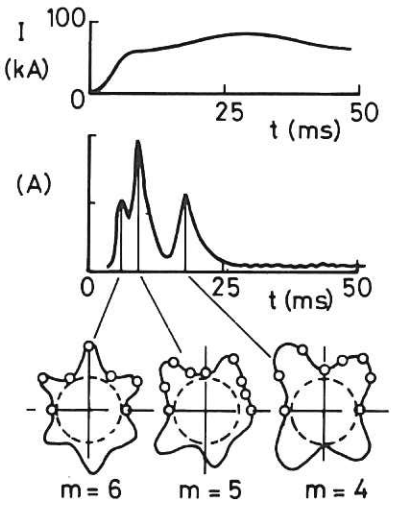

Mirnov oscillations T-3

Fig.10 Mirnov oscillations T-3.

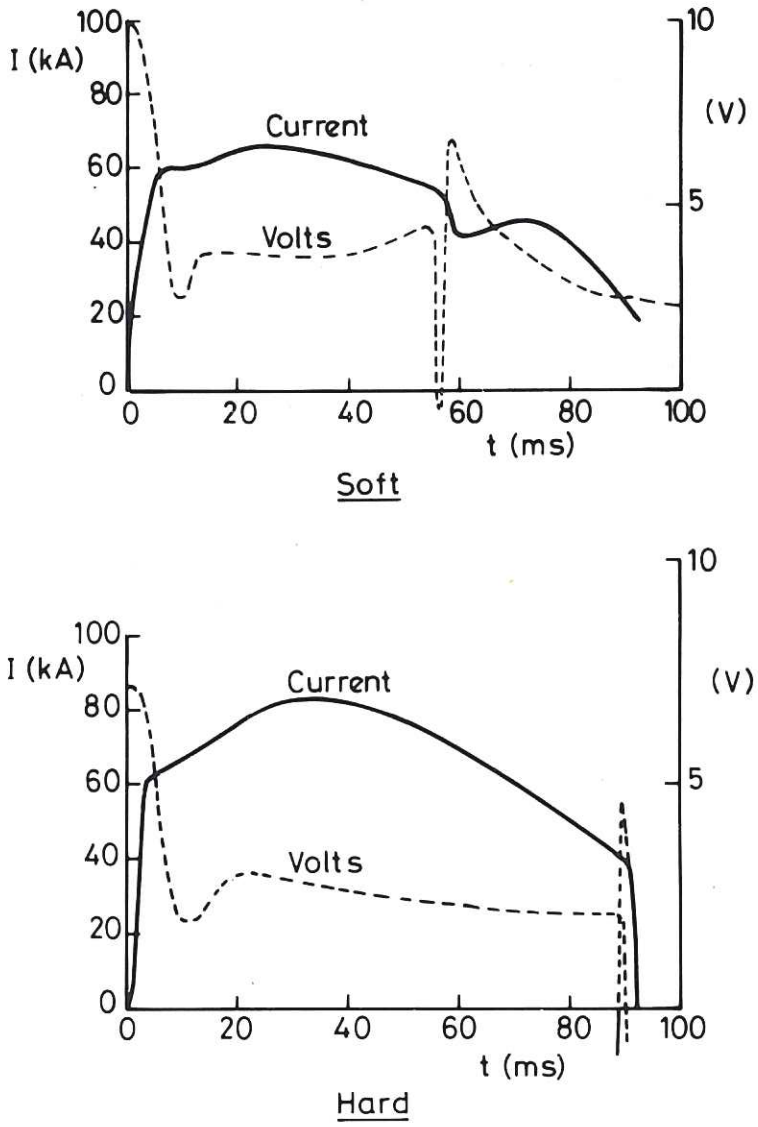

Fig.11 Pulsator disruptions.

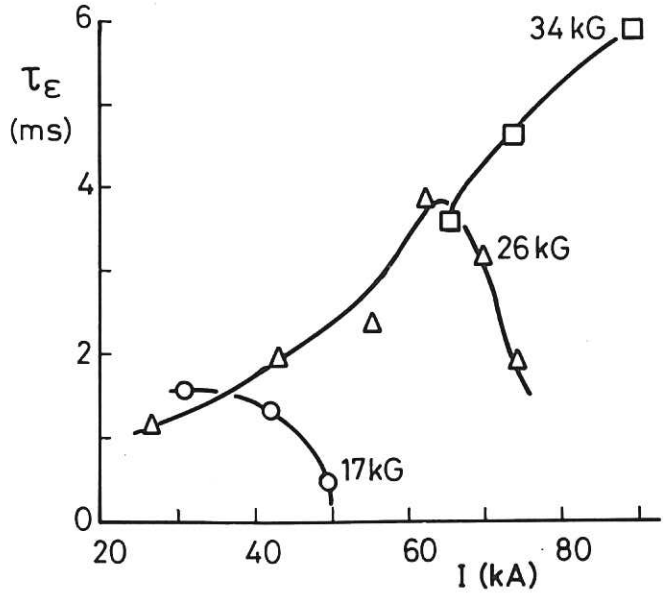

Fig.12 Energy containment time vs discharge current T-3 Tokamak.

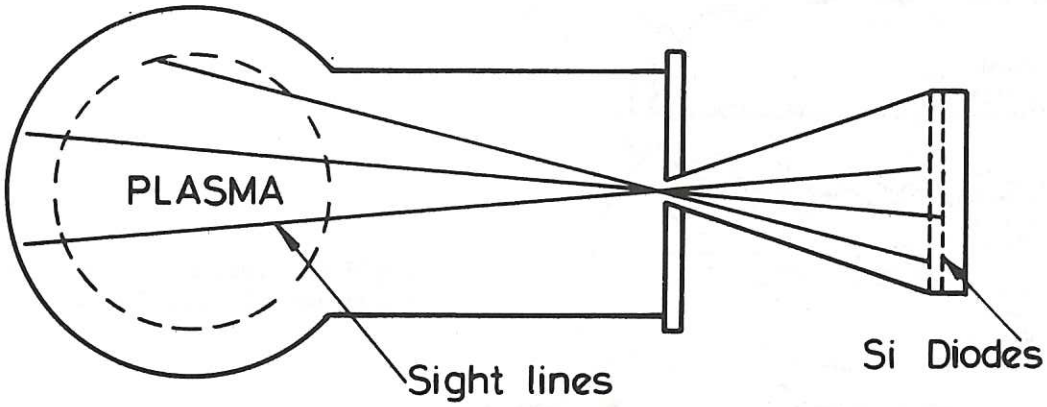

Soft X-ray measurements

Fig.13 Soft X-ray measurement.

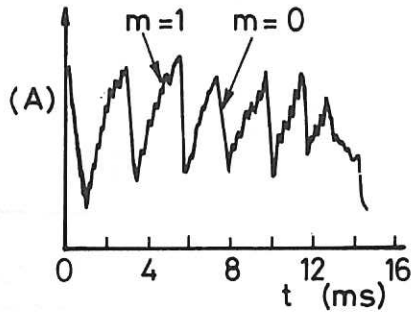

X-ray signals TFR

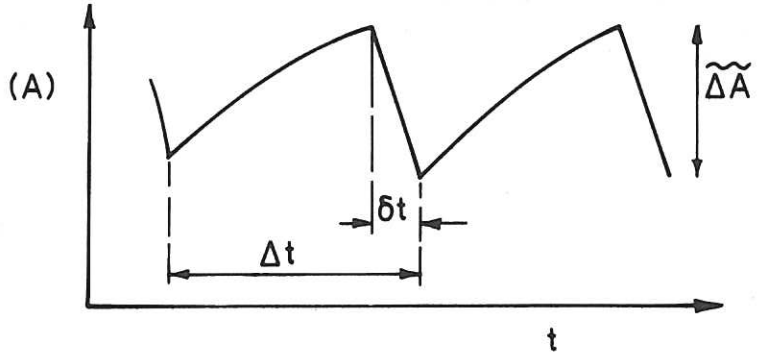

Fig.14 X-ray signals TFR.

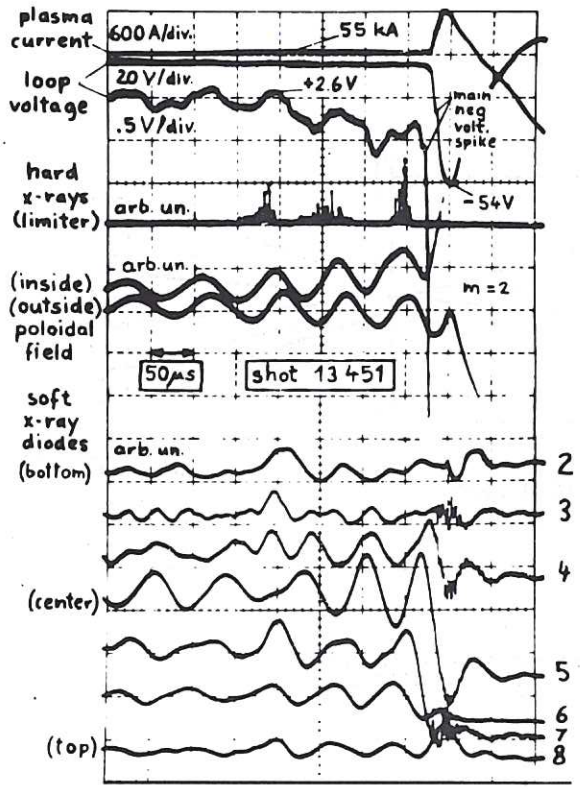

Fig.15 Oscillogram showing approximately the last half millisecond before disruption. (Pulsator).

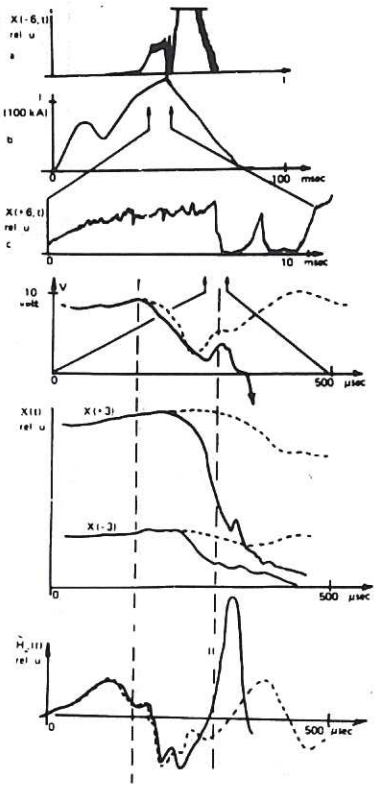

Fig.16 (a) Oscillograms of X-ray radiation X(-6,t) and discharge current 1(t) with total scanning time of 100ms. (b) Oscillogram of X-ray signal with scanning times of 10ms. (c) Fast scans of disruption. Dashed curves show case of predisruption not transformed into disruption. (T-4).

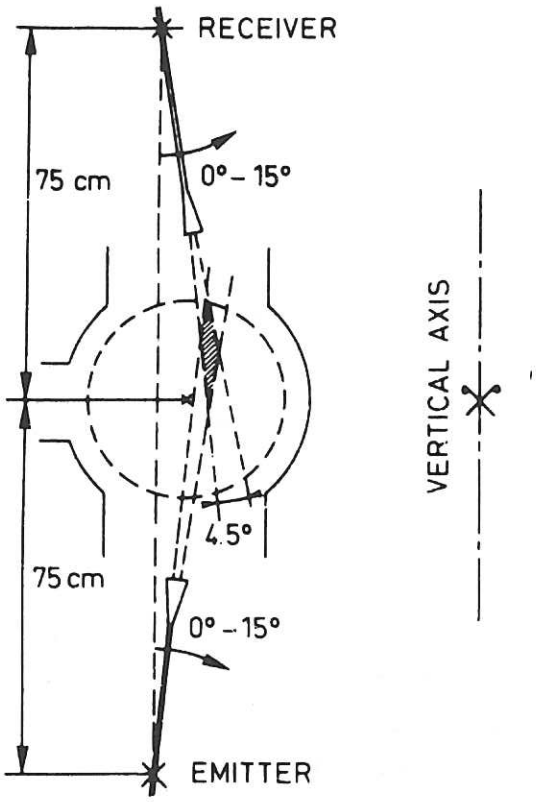

Fig.17 Experimental apparatus for microwave scattering ($\lambda_o \sim 2$mm); $k_o = 28.5\ cm^{-1}$; $k_1 - k_{o/\|} \sim 0$). (TFR).

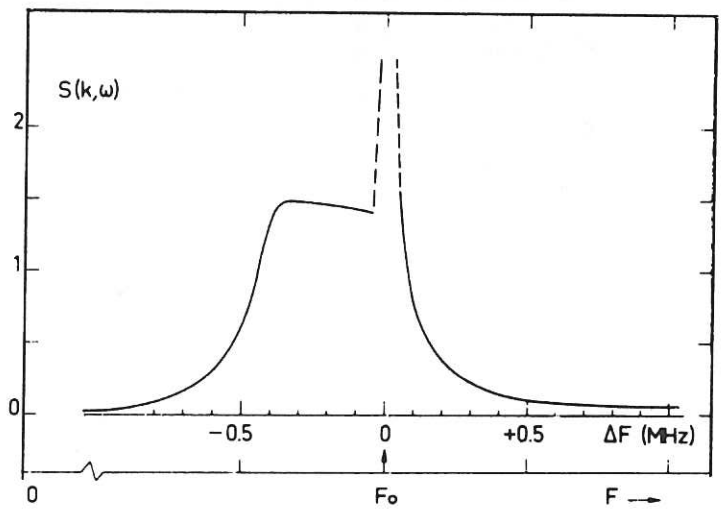

Fig.18 Power scattered by density fluctuations as a function of their frequency during quasi-stationary phase of discharge ($k_{\|} < 1.5\,cm^{-1}$; $k_t \simeq 3\,cm^{-1}$; $r \simeq 15$cm; $k_\theta \simeq 10\,cm^{-1}$; F_o = source frequency (TFR).

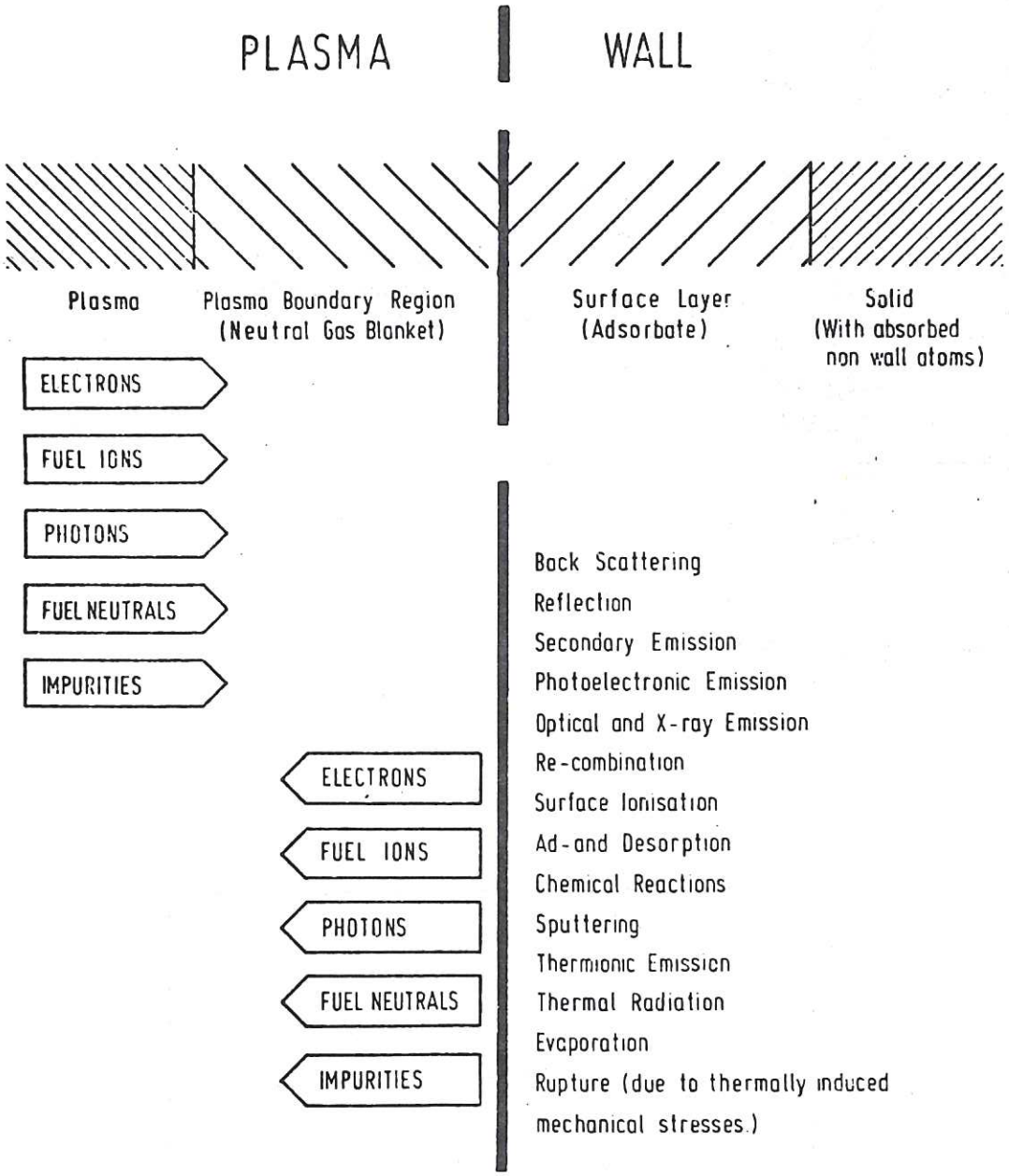

Fig.19 Transition regions (schematic) between plasma and solid and list of elementary processes occurring at the wall.

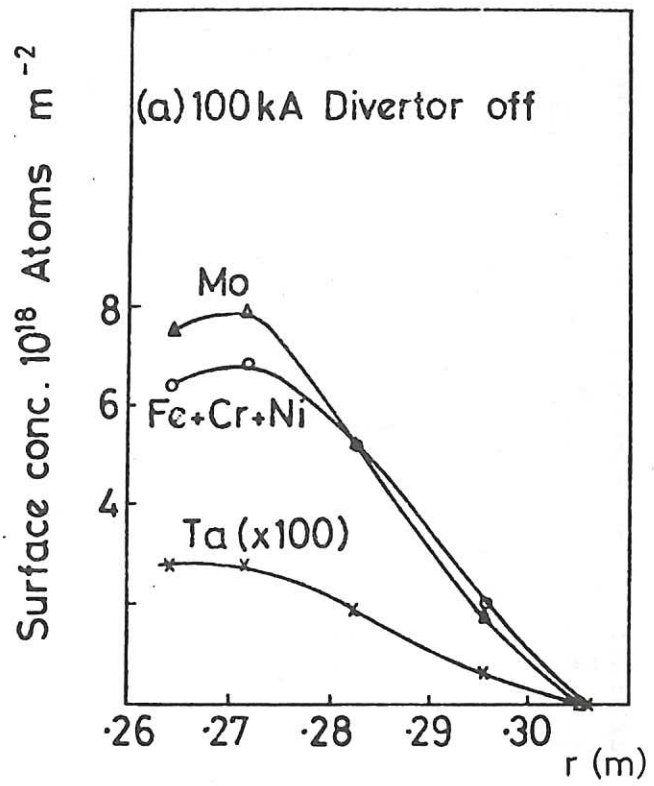

Fig.20 Radial distribution of metal impurities deposited on a probe in DITE discharges.

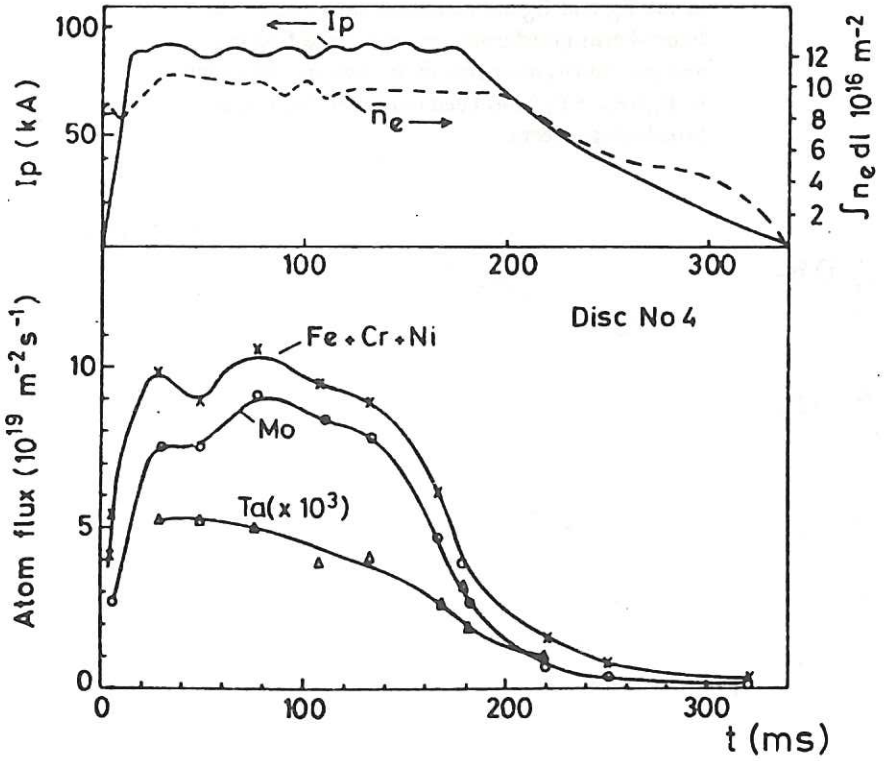

Fig.21 Time distribution of metal impurities arriving on a probe at 0.26m minor radius during a 90kA discharge in DITE (divertor off).

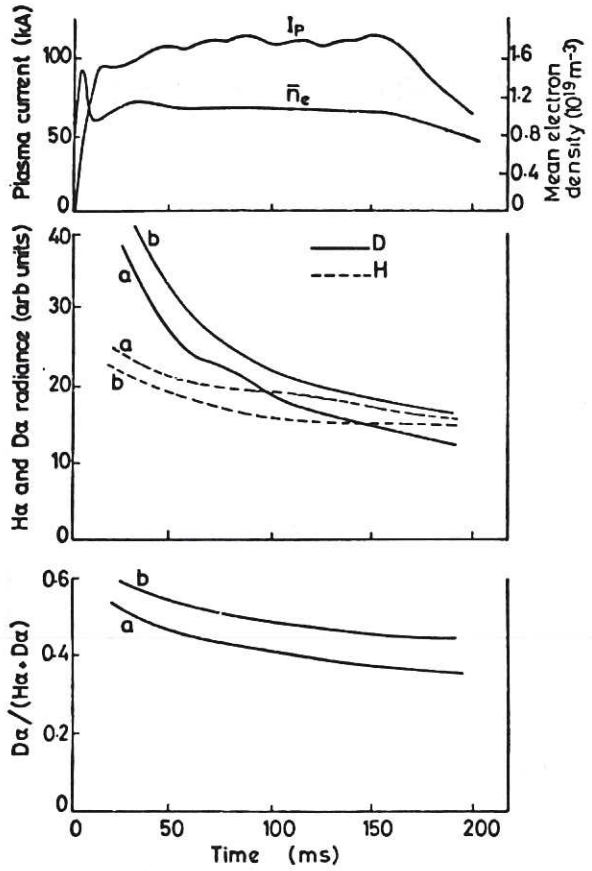

Fig.22 100kA discharges in deuterium in DITE following many in hydrogen. The line intensities of the H_α and D_α are measured with a scanning Fabry-Perot interferometer during the first (a) and second (b) discharge in deuterium. The ratio of $D_\alpha/(H_\alpha + D_\alpha)$ has been corrected for Doppler broadening effects.

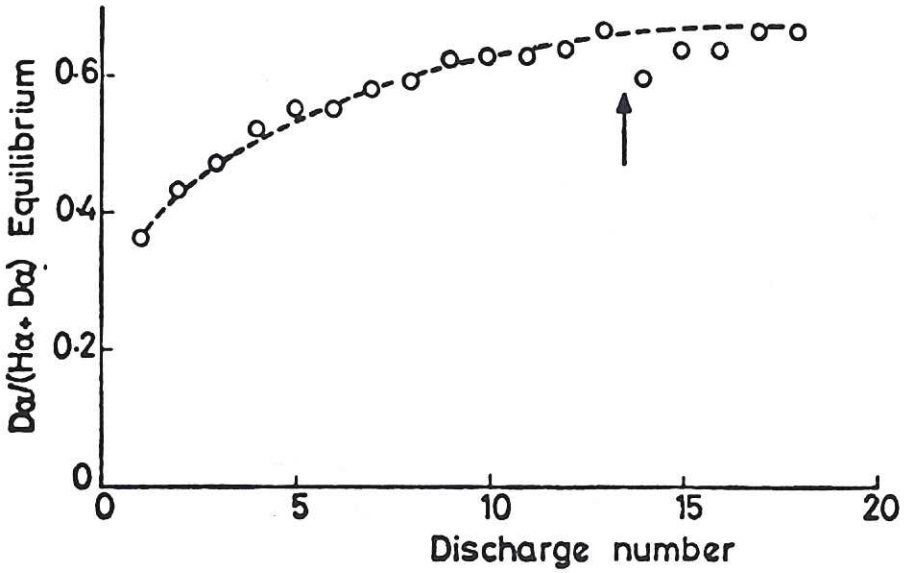

Fig.23 Fabry-Perot measurements of the equilibrium $D_\alpha/(H_\alpha + D_\alpha)$ ratio in successive shots in DITE after the changeover to deuterium filling. The dotted line is the theoretical model. The time between the discharges is normally 5 min but the arrow denotes a delay of 75 min.

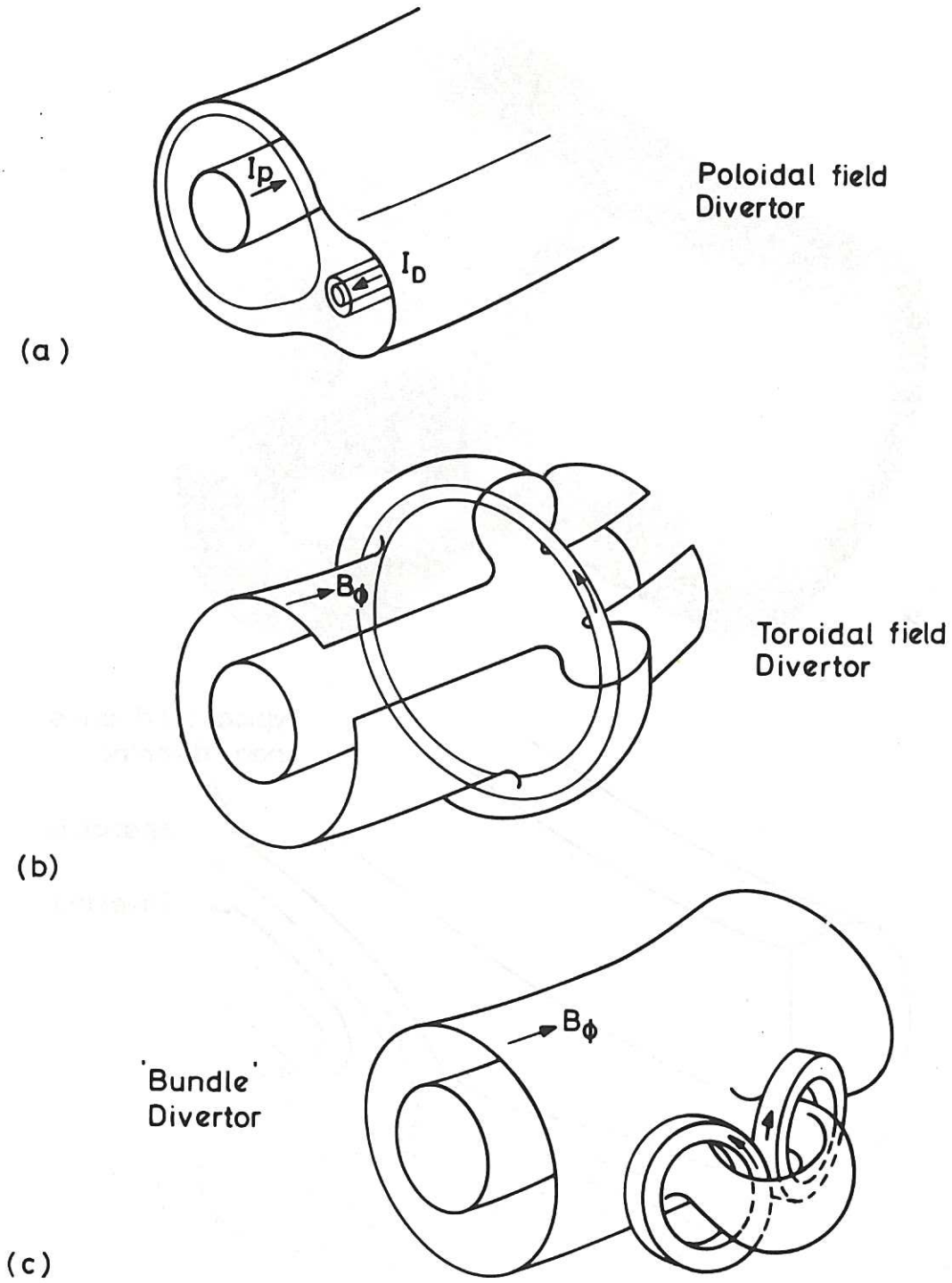

Fig.24 (a) Schematic diagram of various types of divertor.

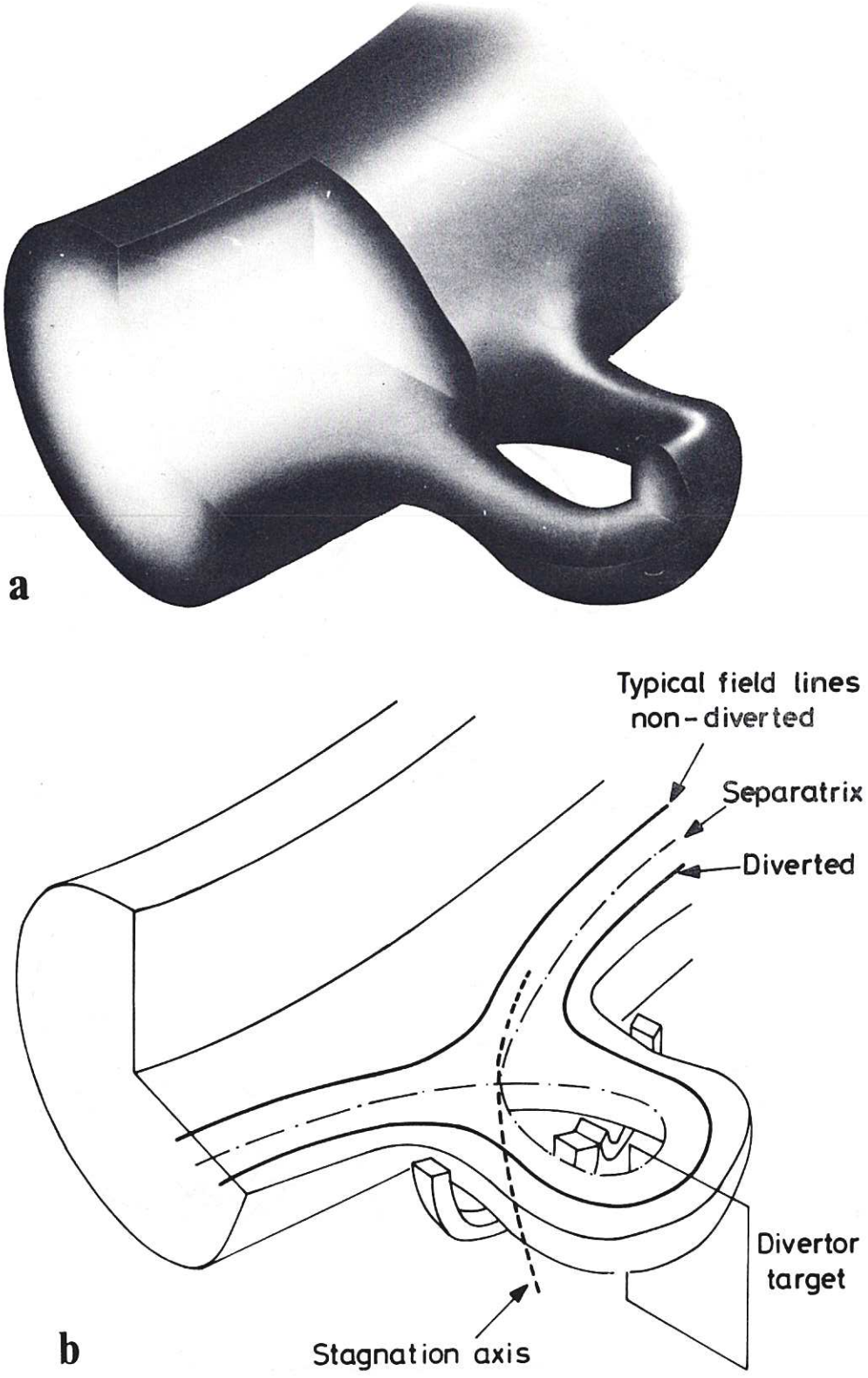

Fig.24 (b) Schematic diagram of idealised bundle divertor.

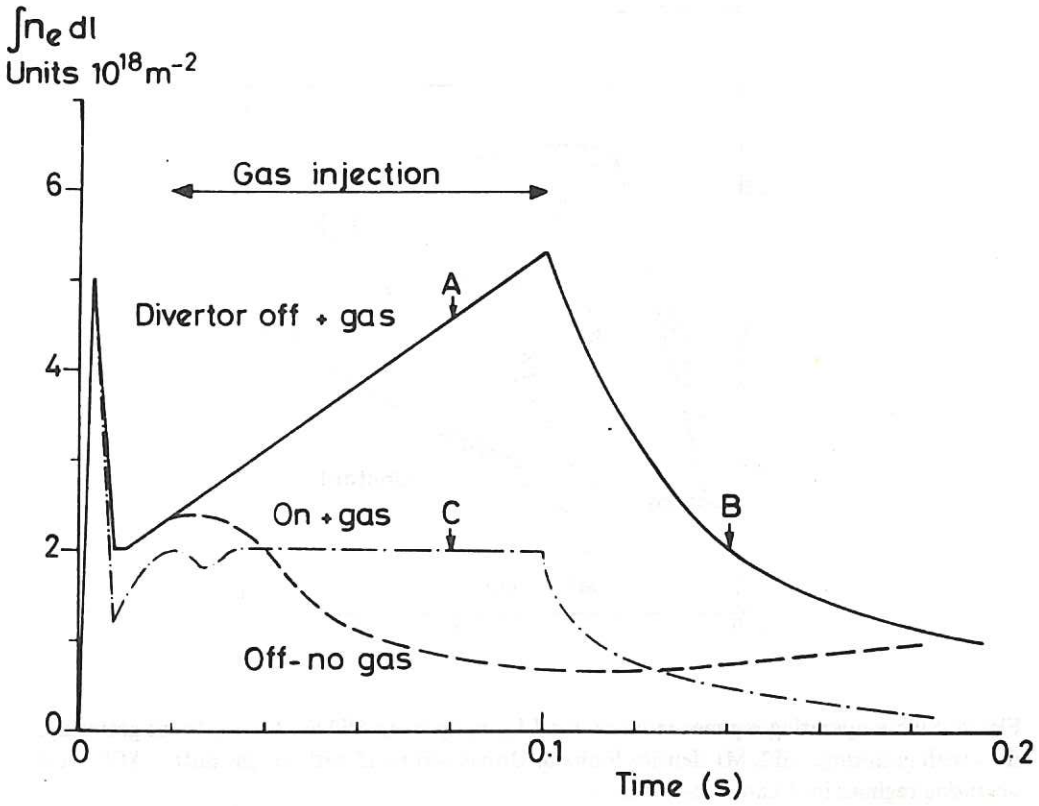

Fig.25 Screening effect of divertor with hydrogen gas feed in DITE.

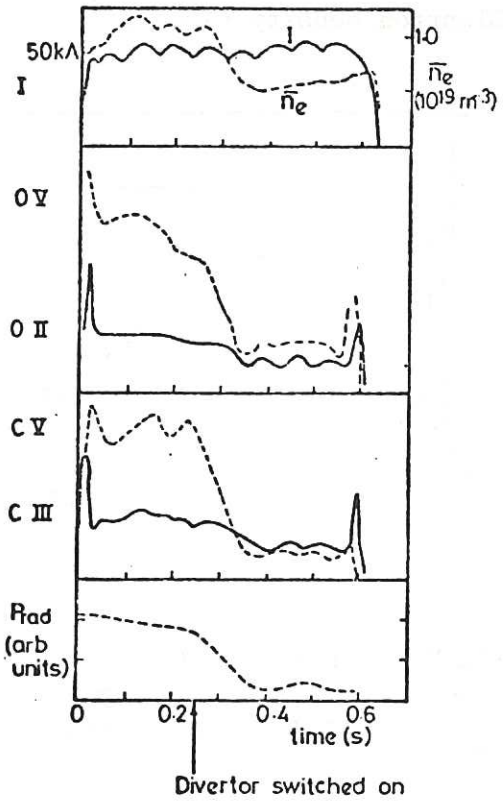

Fig.26 Behaviour of density and radiation for mid-pulse operation of the divertor in DITE.

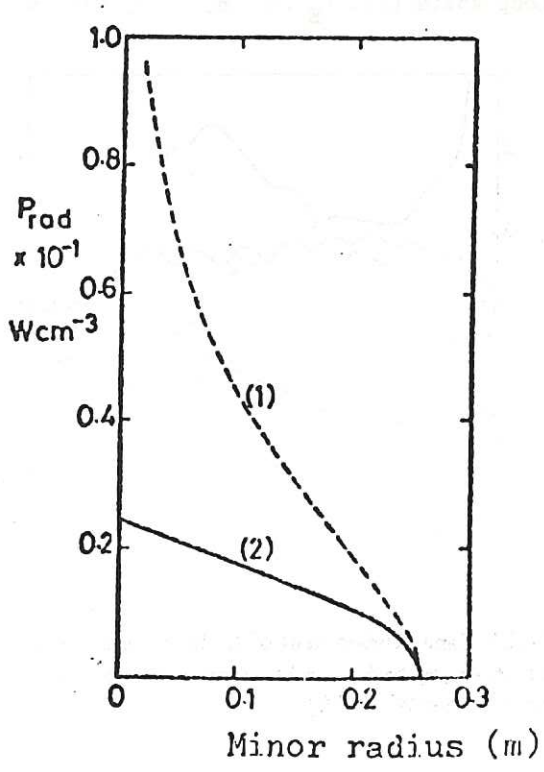

Fig.27 Radial profiles of radiated power from similar discharges (1) undiverted and (2) diverted in DITE.

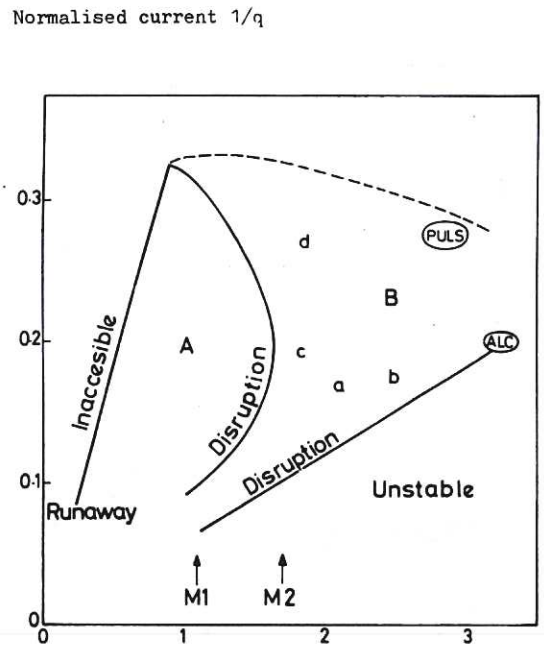

Fig.28 Stable operating regimes in normalised I_p, n_e space in DITE. A. – without gettering, B. – with gettering. M2, M1 density limits in Ormak with and without gas puff. ACL, PULS operating regimes in Alcator and Pulsator.

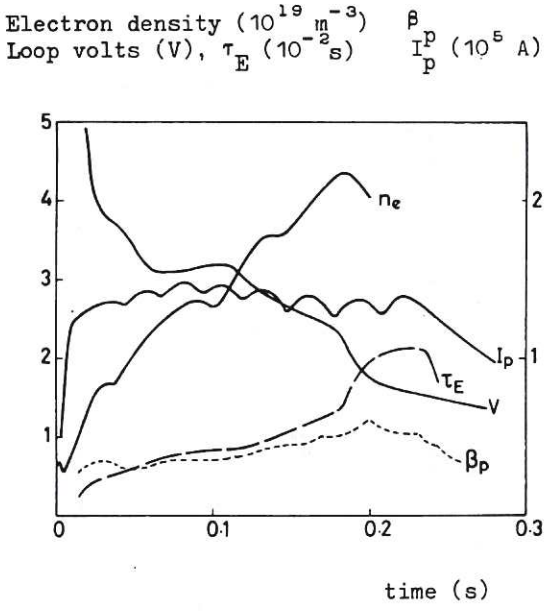

Fig.29 Time development of I_p, loop volts (corrected for dI_p/dt) n_e and β_p and τ_E from a diamagnetic loop for discharge 'b' (DITE).

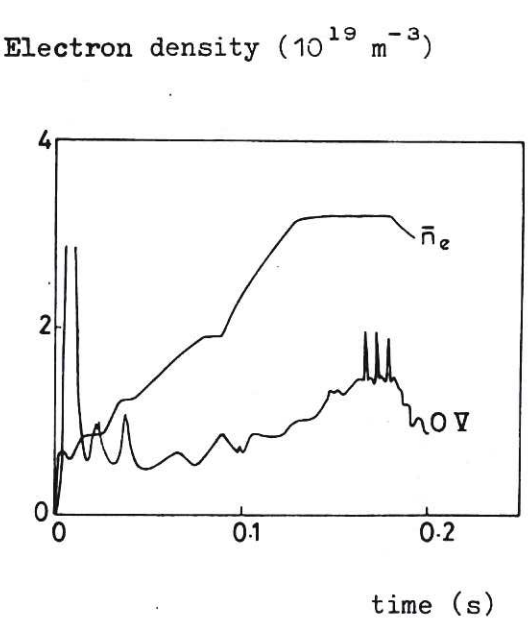

Fig.30 Time development of mean density and intensity of OV(2781 Å) showing bursts of increased oxygen influx during density pauses (DITE).

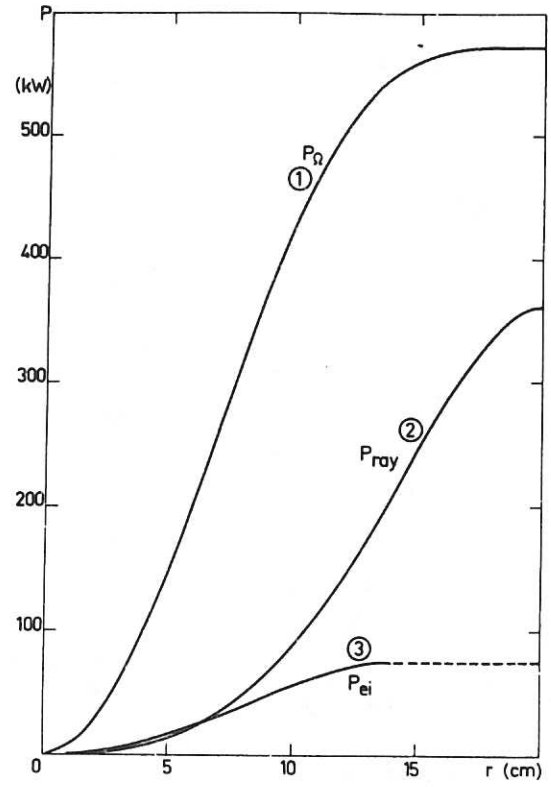

Fig.31 Profile of power contained inside a volume limited by radius r. (1) Ohmic power; P_Ω; (2) P_{ray} = radiated power = bolometric power – charge-exchange power; (3) power given by electron to ions P_{ei}. (TFR)

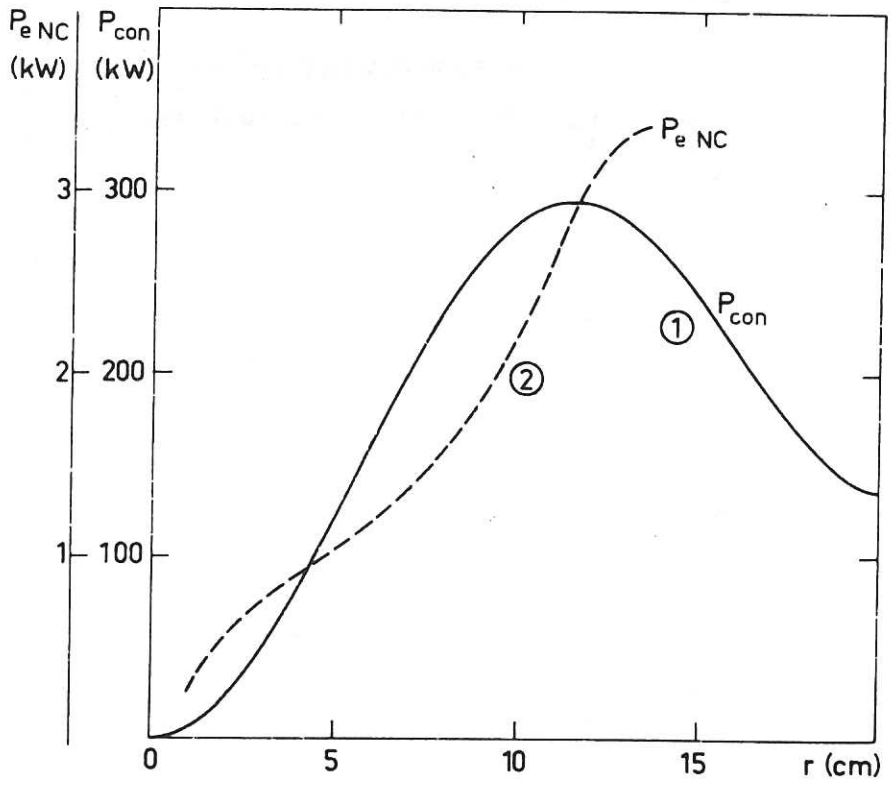

Fig.32 Power lost by conduction and convection inside a volume limited by radius r. (1) experimental; $P_{e\ con}$; (2) neoclassical calculation: $P_{e\ NC}$. (TFR)

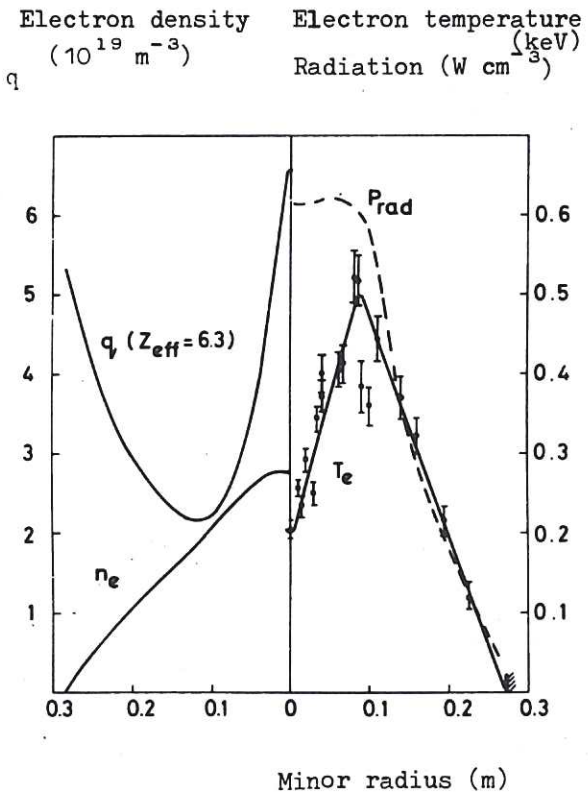

Fig.33 Profiles of T_e, n_e, q and radiated power in DITE.

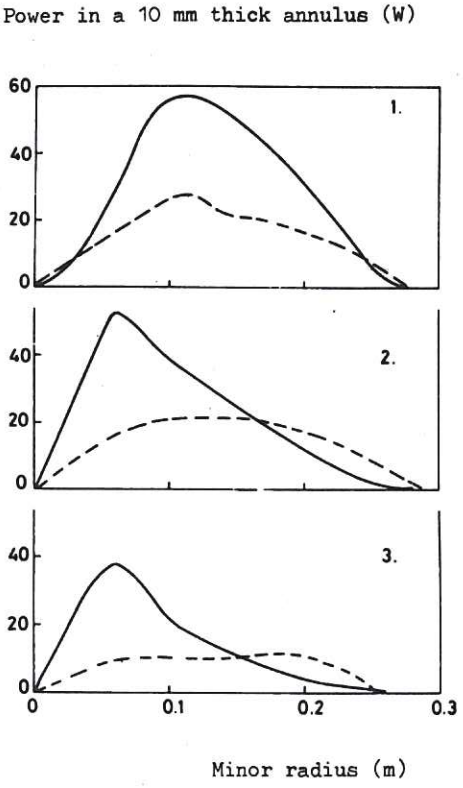

Fig.34 Profiles of ohmic power input (solid line) and power radiated (broken line) in DITE.

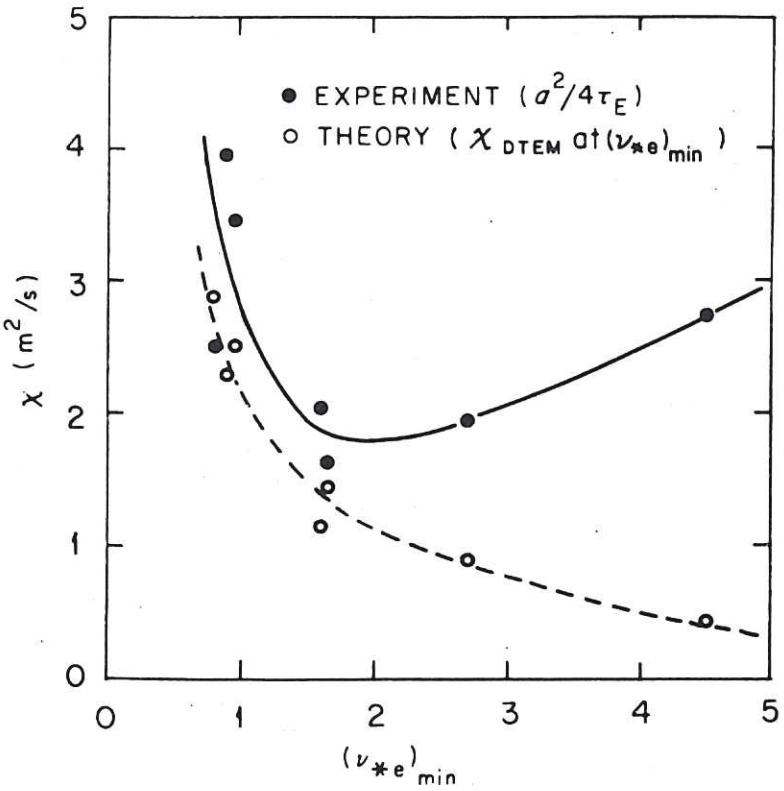

Fig.35 Gross electron thermal conductivity and the estimate from the dissipative trapped electron mode theory as a function of the minimum collisionality parameter $(\upsilon_{oe})_{min}$ in the current scan. (ORMAK)

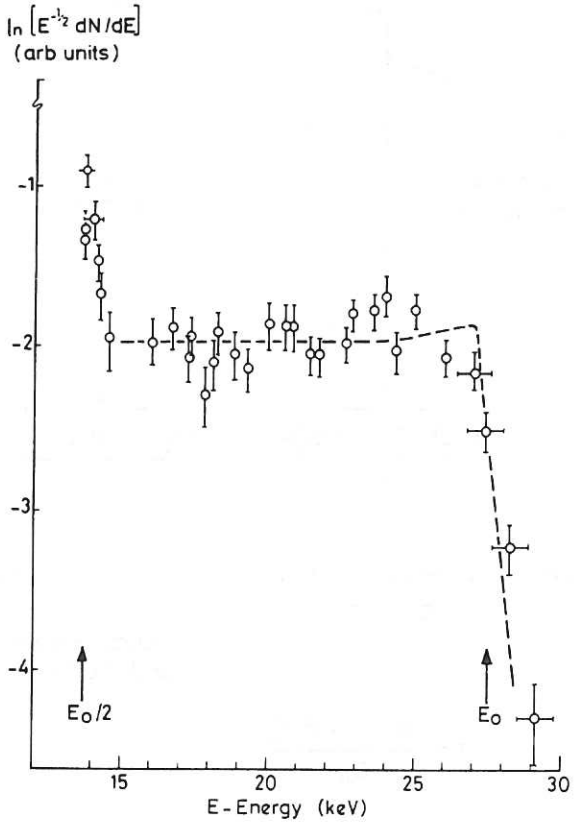

Fig.36 Fast-ion spectrum of 200kW into a 150kA discharge in DITE. (Theoretical curve dashed).

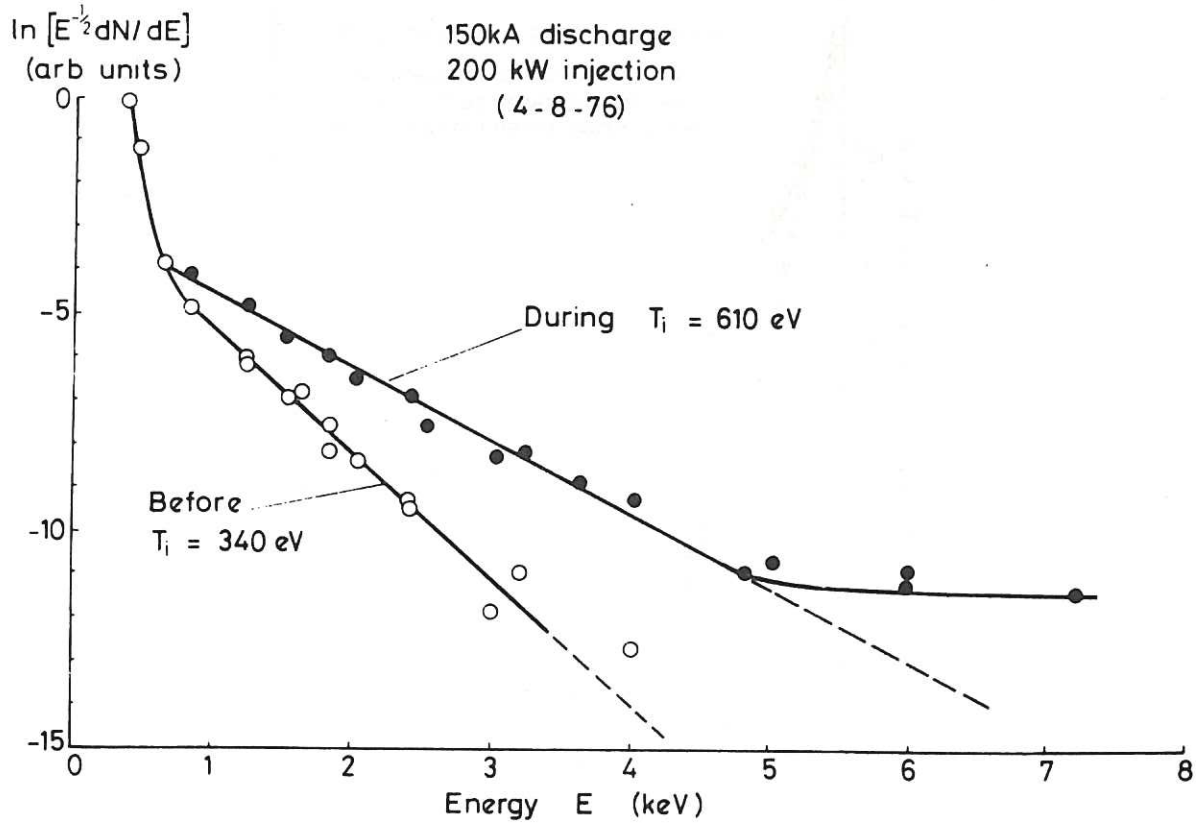

Fig.37 Thermal-ion spectrum for 200kW into a 150kA discharge in DITE.

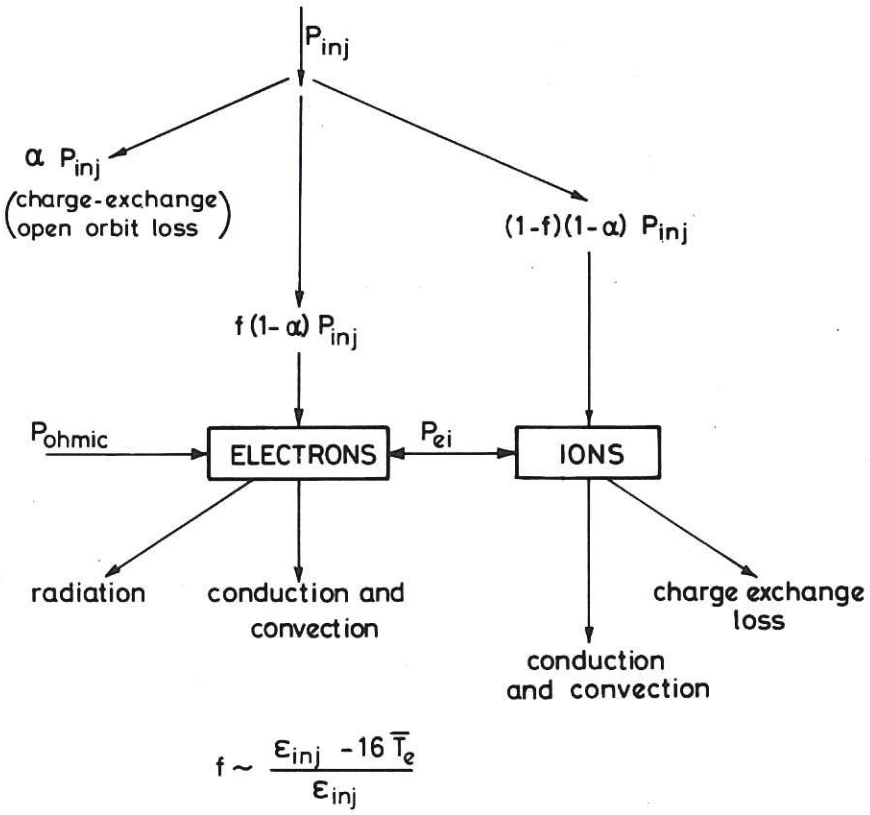

Fig.38 Neutral injection – power flow.

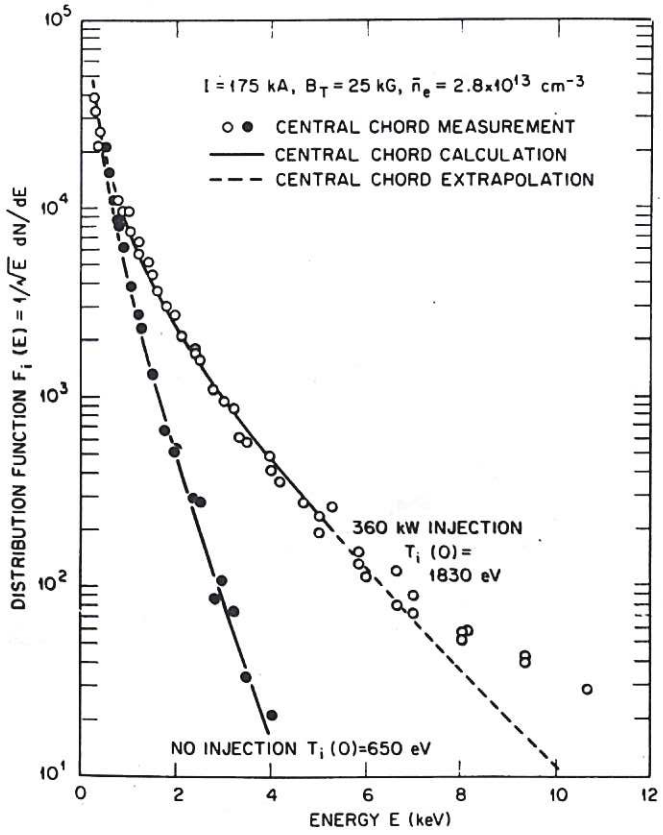

Fig.39 Comparison of perpendicular charge-exchange data with the modelled ion energy distribution for no-injection and 360kW injection cases. (ORMAK)

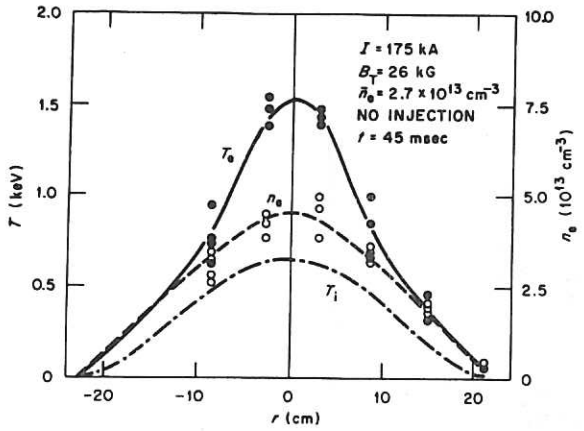

Fig.40 Profiles of electron temperature, electron density and ion temperature for a typical discharge without injection. (ORMAK)

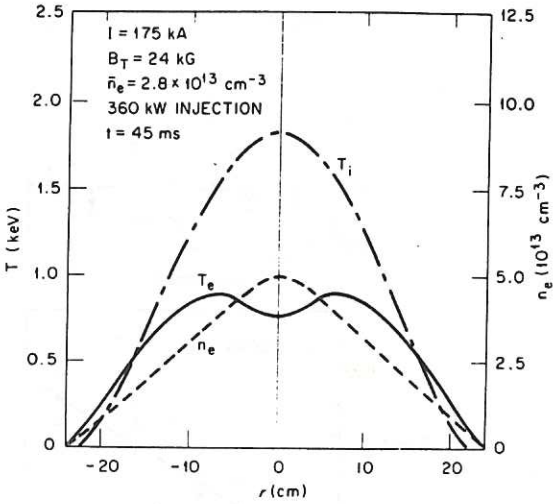

Fig.41 Profiles of ion temperature, electron temperature and electron density for a typical discharge with injection. (ORMAK)

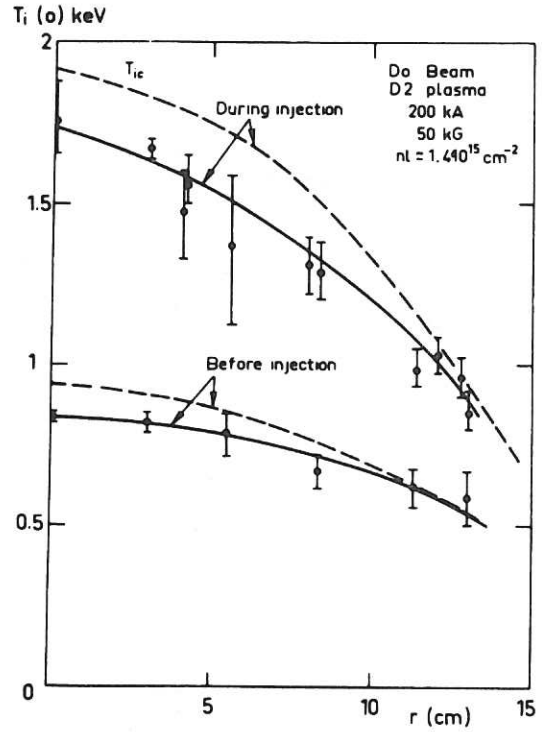

Fig.42 Radial distributions of T_i. The dashed curves give the profiles when plasma attenuation is taken into account (TFR).

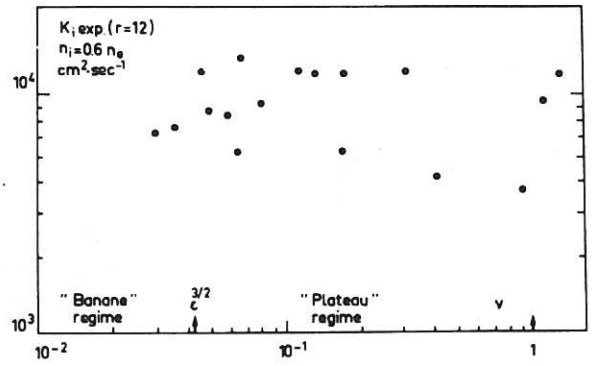

Fig.43 Variation of $K_{i\,exp}$ as a function of the collision frequency (TFR).

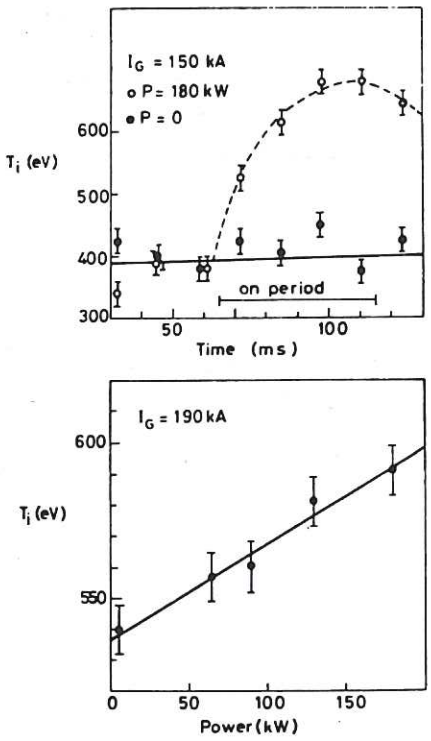

Fig.44 (a) Time dependence of ion temperature in DITE. (b) Dependence of T_i on neutral injection power in DITE.

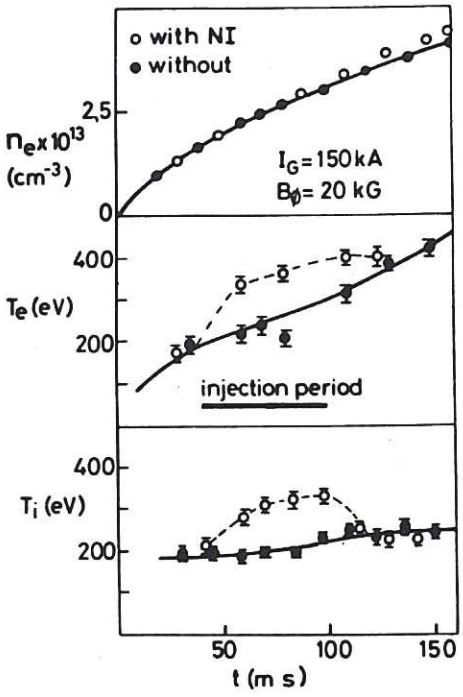

Fig.45 Time dependence of the following quantities in DITE: (a) electron density, (b) central electron temperature, (c) ion temperature. Injectors are on between 40 and 110ms.

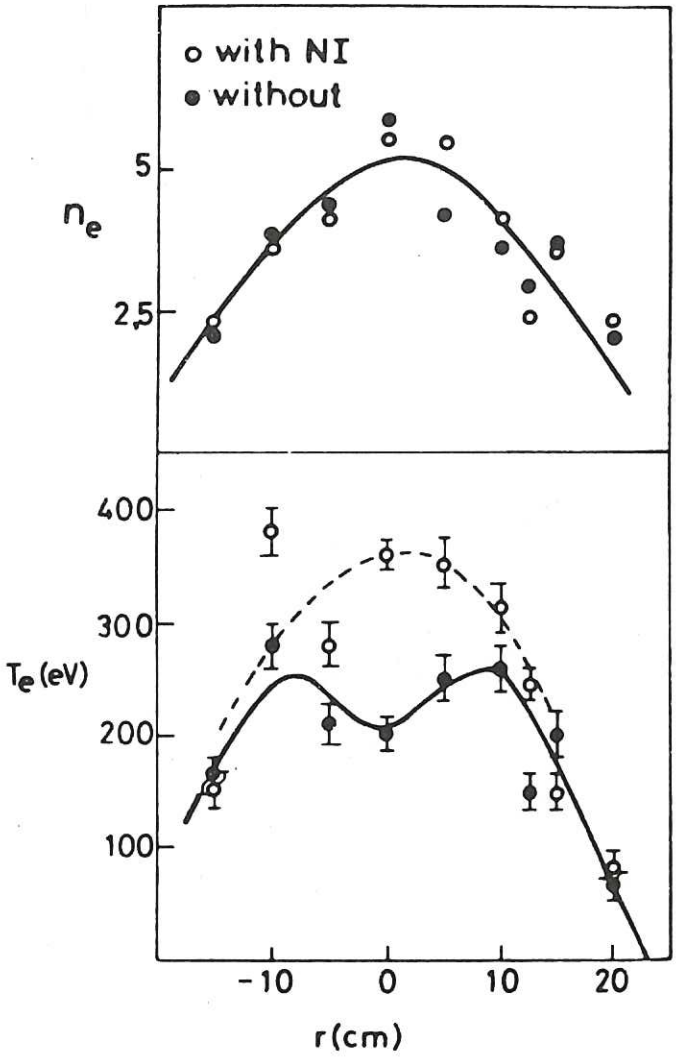

Fig.46 Electron density and temperature profiles at t = 80 ms. n_e is in arbitrary units. (DITE)

HER MAJESTY'S STATIONERY OFFICE

Government Bookshops

49 High Holborn, London WC1V 6HB
13a Castle Street, Edinburgh EH2 3AR
41 The Hayes, Cardiff CF1 1JW
Brazennose Street, Manchester M60 8AS
Wine Street, Bristol BS1 2BQ
258 Broad Street, Birmingham B1 2HE
80 Chichester Street, Belfast BT1 4JY

Government publications are also available through booksellers